Finger Pad Interfacial Pressure Measurement with Fine Spatial Resolution

by

Louis H. Buell Jr.

B.S. Mathematics, Morehouse College, 1999
B.S. Electrical Engineering, Georgia Institute of Technology, 1999

Submitted to the Department of Electrical Engineering and Computer Science
in Partial Fulfillment of the Requirements for the Degree of

Master of Science in Electrical Engineering and Computer Science

at the
Massachusetts Institute of Technology
February 2003

Author…………………………………………………………………………………
Department of Electrical Engineering and Computer Science
January 17, 2003

Certified by……………………………………………………………………………
Dr. Mandayam A. Srinivasan
Senior Research Scientist
Thesis Supervisor

Accepted by……………………………………………………………………………
Arthur C. Smith
Chairman, Committee on Graduate Students
Department of Electrical Engineering and Computer Science

Finger Pad Interfacial Pressure Measurement
with Fine Spatial Resolution

by

Louis H. Buell

Submitted to the Department of Electrical Engineering and Computer Science
on January 17, 2003, in Partial Fulfillment of the
Requirement for the Degree of Master of Science in
Electrical Engineering and Computer Science

ABSTRACT

The sense of touch aids humans in grasping objects, sensing surface texture, and discerning shape. The surface pressure distribution of the finger pad is a critical input to the human tactile system for all of these purposes. In this study we used a sensor with fine spatial resolution to explore the relationship between the surface pressure distribution and the shape of objects contacting the finger pad. Effects of object curvature and net force were studied. Deconvolution, a signal processing technique, was used to increase the spatial resolution of the empirical data.

A pressure measurement system was designed and built to investigate the surface pressure of the finger pad. The behavior of the pressure sensor was examined to provide a clearer idea of it limitations. Drift, manual positioning error, linearity, anisotropy, inter-element variability, and spatial response profile were all studied. We showed that the sensor readings are approximately linear, anisotropic, and that the gain for each element of the sensor is different. The spatial response profile was measured and the sensor was calibrated in order to convert voltages to pressures.

The surface pressure was measured from subjects when cylindrical objects of different sizes were indented onto the finger pad. The spacing between samples was studied to see if smaller step size between measurements produced better results. The correlation between pressure distribution and the fingerprint was also studied. Dips in surface pressure roughly corresponded to grooves in the fingerprint, though these features were at the limit of the spatial resolution of the sensor. The pressure records were compared with the pressure distribution predicted by Hertz theory. Hertz theory was found to model the observed pressure distribution reasonably well, though it failed to account for observed anisotropy due to the non-spherical shape of the finger pad, and pressure concentration due to finger ridges.

Due to the limited spatial resolution of the pressure sensor, deconvolution was investigated. Deconvolution was found to increase the spatial resolution of pressure

measurements, but not enough to fully resolve pressure concentration due to individual finger ridges. This was most likely due sensor noise and the complexity of the spatial response profile of the pressure sensor.

Thesis Supervisor: Dr. Mandayam A. Srinivasan
Title: Senior Research Scientist

Contents

1.0 Introduction

1.1 Overview

The human body has the ability to interact with the outside world through the use of five sensory systems: touch, sight, sound, smell and taste. The information received from these senses is important for human beings to function, and undoubtedly, touch plays a significant role in many aspects of life. This sense is activated by the exertion of pressure or surface tractions on the skin. The tactile sense aids humans in gathering information about the shape, size, temperature and texture of objects. Furthermore, this sensory system allows humans to manipulate or grasp objects and to feel pain or pleasure. Although researchers have a comparatively advanced understanding of how humans see and hear, little is understood about the complex mechanisms involved in touch.

While scientists know that touch receptors are located throughout the skin and are constantly supplying information about surrounding environments, further research is necessary to establish a complete knowledge of the mechanics involved in touch. As a result, the primary goal of this research project is to provide a clearer understanding of the biomechanics of the human tactile system and how humans perceive objects through touch. We know that the following events take place during a human's perception of an object through touch: 1) an object comes into contact with the finger resulting in a distribution of forces on the surface of the skin; 2) the surface force distributions lead to internal mechanical stresses and strains; 3) the mechanoreceptors in the skin transduce the stresses and strains into neural impulses; and 4) the object is perceived when neural impulses reach and are decoded by the brain [Raju and Srinivasan, 1999]. Figure 1-1 illustrates these steps.

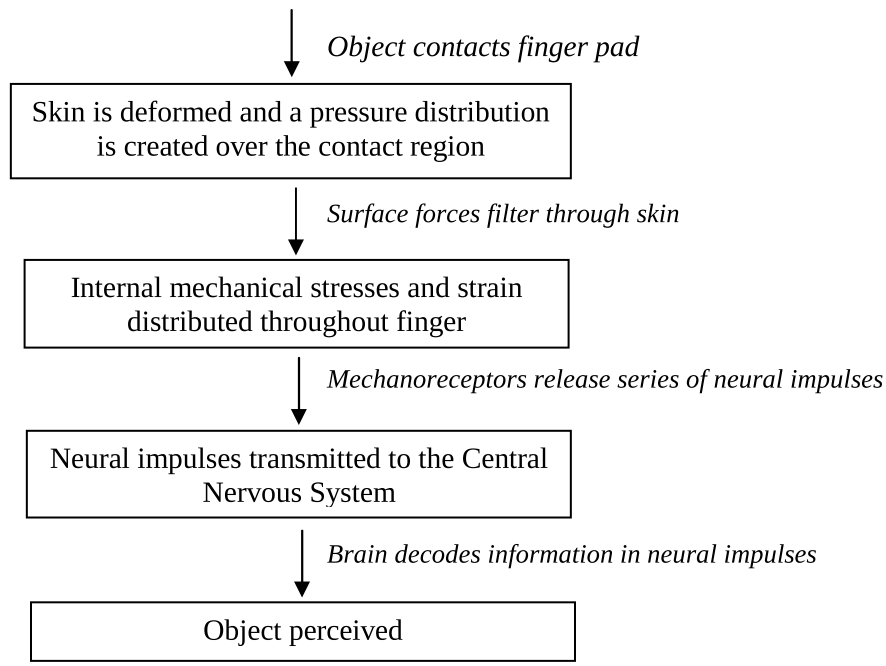

Figure 1-1. The events that take place during a human's perception of an object through touch.

1.2 Motivation

This study will focus on measuring the pressure distribution on the surface of the finger when it comes in contact with an object, the first step of Figure 1-1. Understanding the relationship between the shape of an object indented onto the finger pad and the resulting surface pressure distribution during touch is essential to understanding how humans perceive an object by touch. A study of the pressure distribution on the surface of the finger pad will give us further insight into the distribution of stresses and strains on the mechanoreceptors.

In previous work, Finite Element Models (FEM) have been used to study the pressure distribution when surfaces of different curvatures are indented onto the fingertip. However, these models need to be verified with empirical measurements to ensure their validity. The present study will allow researchers to compare our empirical measurements with FEM predictions of surface traction and thus adjust the model parameters to better reflect reality. This will allow us to check a step in the tactile sensing transduction pathway that we have only been able to model so far. Thus, our study will provide further fundamental scientific understanding of the origins and mechanisms of tactile information.

Another long term goal of our study of fingertip pressure distribution is to aid in the development of tactile sensors for hand and arm prostheses that will give the user a sense of touch. This research can also allow researchers to improve tests to evaluate tactile sensibility of normal and impaired hands. Understanding the pressure distribution will also provide insights for the design and development of tactile sensors for dexterous robots which perform human-like functions in unstructured environments.

1.3 Thesis Overview

This thesis is organized as follows: Background information about the anatomy of the finger as well as previous research about the biomechanics of the human tactile system are presented in Chapter 2. Chapter 3 describes the experimental setup and the pressure sensor used to collect pressure measurements. The results of measuring the pressure distribution of the finger pad are introduced in Chapter 4. Chapter 5 concludes the paper with a summary of the results.

2.0 Background

2.1 Human Fingertip

The human finger tip is comprised of bone, nail, blood vessels, fat, nerves, sweat glands and skin. The skin of the human finger pad is made of an epidermis and a dermis layer. The epidermis is the outer layer of the body that protects it from the outside environment. It is comprised of a number of layers: stratum corneum, stratum lucidum, stratum granulosum, malphigian layer, and stratum basale [Tubiana, 1981]. The upper-most layer of the epidermis is made up of dead skin cells that are easily removed, and a series of ridges that make up the fingerprint are located on the surface of the epidermis. The dermis is located below the epidermis and protects and cushions the body. It houses sweat glands, hair follicles, blood, lymph vessels and nerve endings. The dermis and epidermis interdigitate in a pattern that mimics the surface ridges on the skin [Lockhart et al., 1965]. Near this interface four types of mechanoreceptors are located: Merkel's disks, Meissner's corpuscles, Pacinian corpuscles, and Ruffini corpuscles [Johansson and Vallbo, 1983]. These mechanoreceptors gather information about the features of objects, and also sense pressure, pain, and temperature.

2.2 Previous Work

Tactile research can be separated into three distinct areas which are biomechanics, psychophysics, and neurophysiology.

Research on the biomechanics of tactile sensing deals with understanding the mechanics of touch, and the resulting stress-strain relationships in the skin, which activate the mechanoreceptors that send neural impulses to the brain. Biomechanical studies involve investigation into the mechanical properties of skin, the surface pressure during contact, and the stress-strain relationship that occurs in the skin.

Philips and Johnson modeled the finger as a homogeneous, linear elastic, isotropic and infinite medium to study the connection between the measures of subsurface strain and neurological readings [Philips and Johnson, 1981b].

Srinivasan proposed the *waterbed model* of the finger, which modeled the finger as an elastic membrane filled with an incompressible fluid. The model could predict the deformation profile on the surface but could not accurately predict the stress-strain relationship within the finger [Srinivasan, 1989].

Dandekar and Srinivasan created a multi-layered FEM model that was able to determine the surface deformation and stress-strain relation during touch [Dandekar and Srinivasan, 1996].

Diane Pawluk studied the dynamic mechanical interaction between the finger pad and a flat indentor applied to the finger pad. Controlled position trajectories were applied to the finger pad and the resulting spatially distributed pressure response and force were measured [Pawluk, 1997].

Cysyk and Srinivasan also created a multi-layered FEM model of the human finger pad. The model was indented with surfaces of various curvatures, while the contact force was held constant until steady state conditions were reached. They found that during indentation, the primary mechanical stimulus across the finger pad was the contact pressure [Cysyk, 1999].

Raju and Srinivasan investigated the mechanics of touch using a multi-layered FEM of a primate finger pad. The problem of computing surface loads from neural responses was addressed. They showed that the surface pressure could be decoded from neural impulses [Raju and Srinivasan, 1999].

2.3 Hertz Theory

Hertz theory of normal contact of elastic solids predicts the shape of the area of contact when two non-conforming solids touch [Johnson, 1985]. This theory of the contact between two elastic bodies applies to homogeneous, isotropic bodies that are much larger than the contact area. When two smooth nonconforming surfaces initially come in contact, they touch at a single point. As the load increases, deformation occurs in the area of that point, the area of contact grows, and so does the distribution and magnitude of surface tractions. During this process, Hertz theory predicts the shape and area of contact, as well as the distribution and magnitude of surface tractions over the surface. We used Hertz theory to predict the surface pressure distribution of the fingertip when it comes in contact with cylindrical objects of various radii.

The relative radius of curvature of the two contacting bodied is given by

$$\frac{1}{R} = \frac{1}{R_1} + \frac{1}{R_2} \tag{2.1}$$

where R_1 is the radius of the finger pad and R_2 is the radius of the contacting object. When the finger and object come in contact, with a known load P, the resulting contact area has a radius of,

$$a = \left(\frac{3PR}{4E^*} \right)^{1/3} \tag{2.2}$$

where

$$\frac{1}{E^*} = \frac{1 - v_1^2}{E_1} + \frac{1 - v_2^2}{E_2} \tag{2.3}$$

E_1 is the modulus of elasticity of finger pad and E_2 is the modulus of elasticity of the object. v_1 is the Poisson's Ratio for the human finger pad, and v_2 is the Poisson's Ratio of the object. If the object is incompressible, then the Poisson's Ratio is assumed to be 0.5. The Poisson's Ratio of the finger pad was assumed to be 0.48.

Assuming that the contact area is circular and has radius *a* and load *P*, then the maximum contact pressure (p_0) is given by,

$$p_0 = \left(\frac{3P}{2\pi a^2} \right) = \left(\frac{6PE^{*2}}{\pi^3 R^2} \right)^{1/3} \tag{2.4}$$

The pressure distribution produced is of the form

$$p = p_0 \left\{ 1 - \left(r / a \right)^2 \right\}^{1/2} \tag{2.5}$$

where *r* is the radial distance from the contact center and $r \le a$.

2.4 Deconvolution of Shift-Invariant Sensor

Ridges, sweat pores, and grooves in the finger print are all features that may have interesting consequences for the mechanics of touch. In order to study the effects of such fine features, measurements with fine spatial resolution are required. Deconvolution is one potential method for increasing the spatial resolution of interfacial pressure measurements.

Deconvolution is the inverse of convolution, a familiar signal processing technique. In deconvolution an input signal *x[n]* is estimated from a measured output signal *y[n]*, when the impulse response *h[n]* of a system is known. Successful deconvolution depends on linearity and shift invariance of the system, as well as low noise, and accurate knowledge of the system impulse response. Figure 2-1 gives a block diagram of the system to be deconvolved in this study. Here the goal is recover the actual finger pad pressure distribution from the measured finger pad pressure distribution, using the spatial response profile of the sensor.

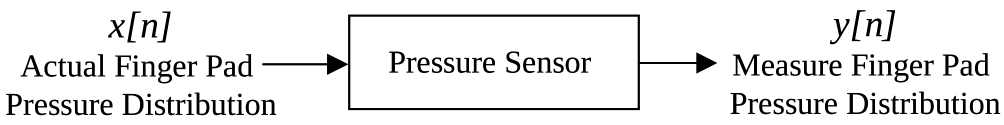

Figure 2-1. Block diagram of the surface pressure measurement of the finger pad.

A shift-invariant system is one in which a shift in the input corresponds to an identical shift in the output. In order for a system to be shift-invariant the curvature of the body must be constant [Raju and Srinivasan, 1999]. Accordingly, we limited our study to indentation by cylindrical stimuli, in which curvature remains constant with shifts in spatial coordinate. A second requirement for shift invariance is that fixed boundary conditions must not be near where shift-invariance is evaluated Accordingly, we made our measurements near the center of the pressure sensor, far from the fixed boundary condition of zero pressure outside the array.

3.0 Finger Pad Pressure Distribution Measurement System

3.1 Experimental Setup

The apparatus designed to measure the surface pressure of the finger pad consists of a motion platform, a load cell, a pressure sensor, various indentors and a personal computer (PC). Figure 3-1 shows the experimental setup. The motion platform consists of two Daedal High Precision Linear Tables each with a Zeta 57 step motor. One axis travels in the *x* while the other axis in the *y* direction in a Cartesian plane. A third Zeta 57 step motor is used for a rotational direction of travel. A Sensotec 1000 gram Model 31 Miniature load cell is used to measure the total net force that was applied to the fingertip. The data from the load cell is collected by a Sensotec Model HM Single Channel Signal Conditioner/Indicator with RS232 input to a PC. Two sets of 500 gram weights are used to counterbalance the mass of the rotational motor against the load cell in order to measure the total net force applied to the fingertip. A highly sensitive tactile pressure sensor is used to measure pressure data from the finger pad, which is then sent through a data acquisition board into the PC. A C++ program was used to control the motion platform and to record data from the load cell and pressure sensor.

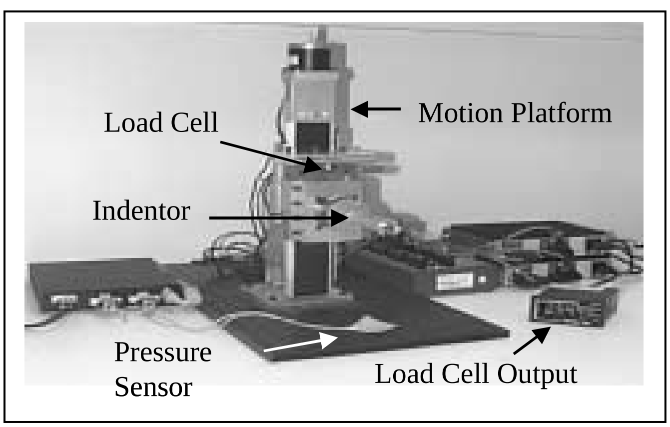

Figure 3-1. Finger Pad Pressure Distribution Measurement System. Consists of highly sensitive pressure sensor, motion platform to control movement of stimulus, load cell to record net force, and various sized interchangeable cylindrical indentors.

Cylinders of various radii were used to indent the fingertip during experiments. The first cylinder had a ½ inch radius while the second had a ¼ inch radius. The conformable pressure sensor was attached to each cylindrical indentor with double sided tape. The subject's hand was supported in a plastic mold with the index finger positioned at 30° from the horizontal, so that the most sensitive part of the fingertip contacted the object. The hand and forearm were constrained and the fingernail was glued to the mold to prevent finger pad movement.

3.2 Pressure Sensor

In order to obtain the surface pressure distribution of the finger pad, we used a highly sensitive tactile pressure sensor developed by Pressure Profile System Inc in Los Angeles, California. The sensor consists of an array 8 elements by 7 elements or 56 total elements; with the size of each element measuring 2 mm by 2 mm. The space between each element is approximately 0.005 inches or 0.127 mm wide. This sensor is conformable and able to fit around various shaped objects. Figure 3-2 shows both sides of the outside of the sensor. The gray side is used as the contacting surface because its response provides less noisy measurements.

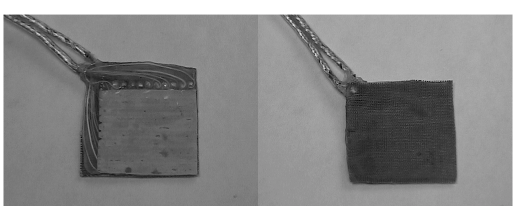

Figure 3-2. Picture of both sides of pressure sensor. The gray side is used as the contacting surface.

The sensor uses capacitive sensing. It is made of a set of parallel strips of copper, which are separated by silicone rubber spaces and orthogonal to another set of parallel strips of copper. The air in-between the two strips of copper is used as a dielectric or a nonconductor of direct electric current. Each intersection of the parallel copper strips constitutes an element. When pressure is applied to the sensor exterior, the copper strips are pressed together, thus increasing the capacitance of the element. This change in capacitance is proportional to the change in pressure above the element [Pawluk, 1997]. Figure 3-3 shows the design of the sensor.

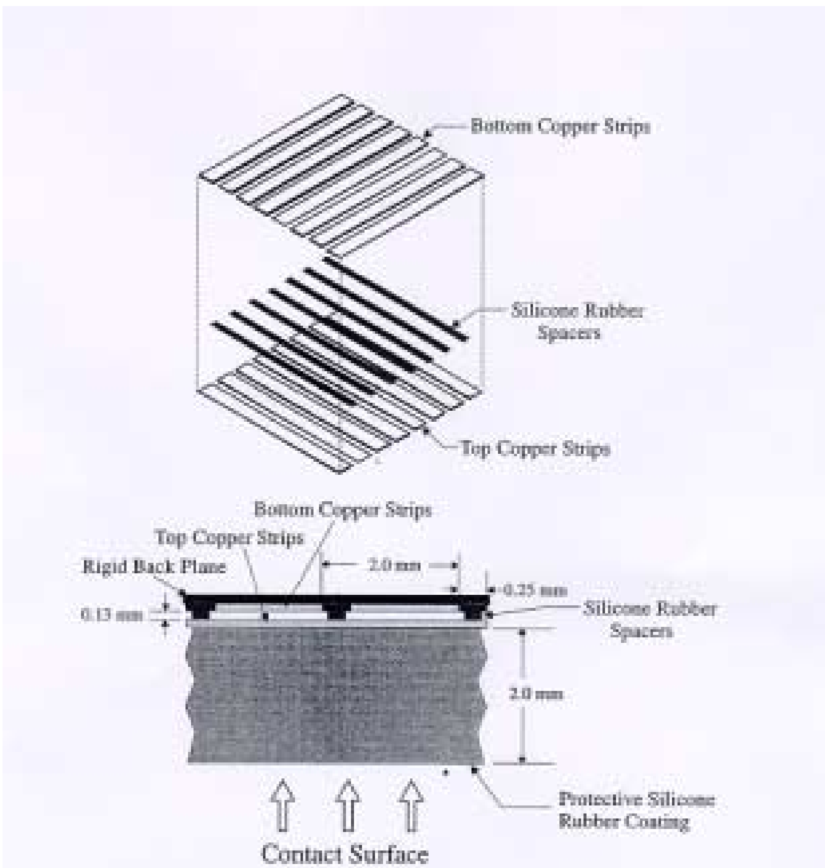

Figure 3-3. Capacitive pressure sensor design [adapted from Pawluk, 1997].

3.3 Sources of Error in Pressure Measurement

We designed several experiments to study the characteristics of the pressure sensor. The characteristics we studied were drift, time dependence, repeatability, linearity, anisotropy, and inter-element variability.

3.3.1 Drift

The pressure sensor was found to exhibit drift in its measurements. Drift was measured over a 10 hour period with the sensor stationary and unloaded. We collected data from the sensor every 30 seconds for 10 hours. Figure 3-4 shows the resulting drift of the sensor. For the first hour, the sensor measurements decrease, and we called this the warm up period for the sensor electronics. During the next three hours the sensor measurements are flat. All experiments that were performed to collect finger pad pressure measurements (see chapter 4) were performed during this three hour time period. In the last 6 hours the sensor measurements steadily increase and we avoided taking finger pad pressure measurements after the four hour mark. In order to account for the drift in our experimental measurements, for each data point, we collected data from the sensor with no load and then data with the prescribed load. We then subtracted the two measurements to calculate the change in voltage or change in pressure.

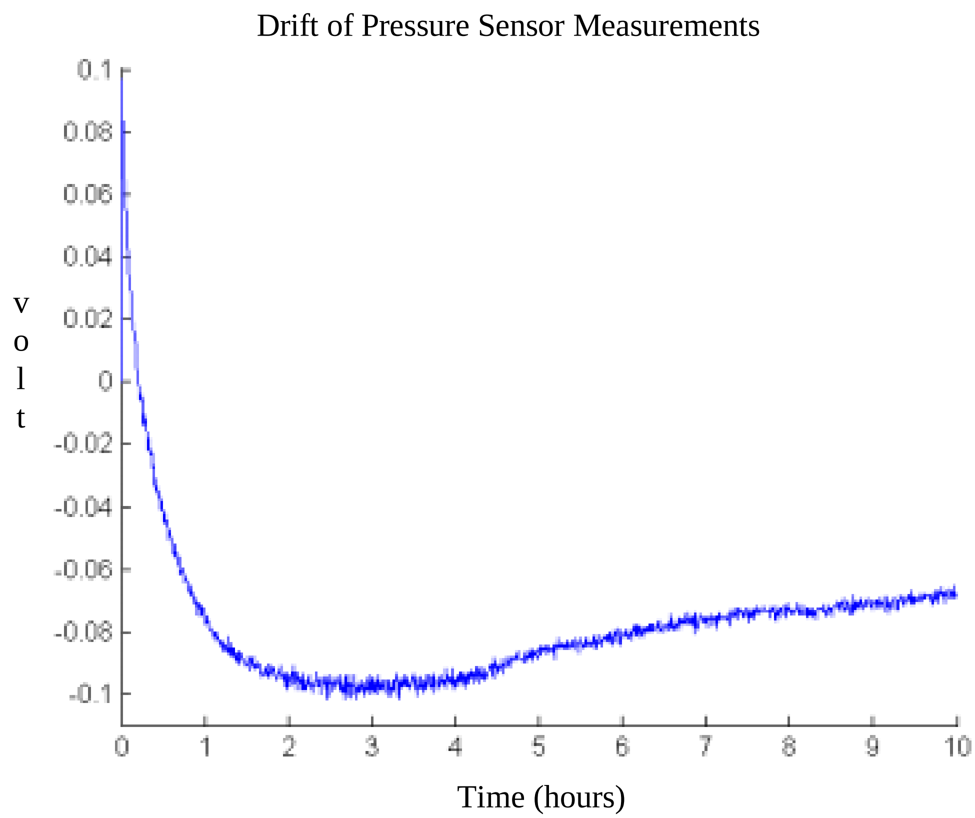

Figure 3-4. Drift of pressure sensor measurements over a 10 hour period.

We next studied the sensor to determine if the measurements of the loaded sensor changed during an experimentally relevant period of 10 minutes. In order to accomplish this, the sensor was laid flat and a stationary object was placed on top of the sensor. Data was read from each element of the sensor once a minute, for a total of 10 minutes. The measurements from each sensor element were compared over the entire time period to assess any changes in the data. We repeated the entire process using a 100 gram (Figure 3-5) and 200 gram weight.

Figure 3-6 shows the response of one row of elements after 10 trials for this given stimulus. The average standard deviation of the seven elements in the row was 0.0028146 or 4.51% of the measurement, and the average range was 0.008643 volts. This minimal change in the response of the sensor indicates the sensor's independence of time over experimentally relevant intervals (10 minutes), when loaded. The two peaks of

Figure 3-6 are different in magnitude because the 100 gram weight overlaid the center of one element, but not to the center of the other.

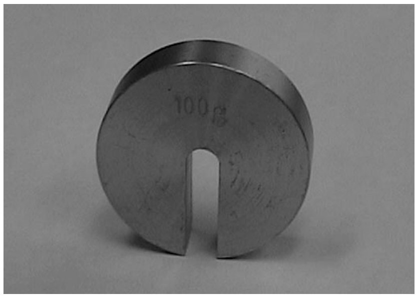

Figure 3-5. 100 gram slotted weight that was applied to sensor in the position shown.

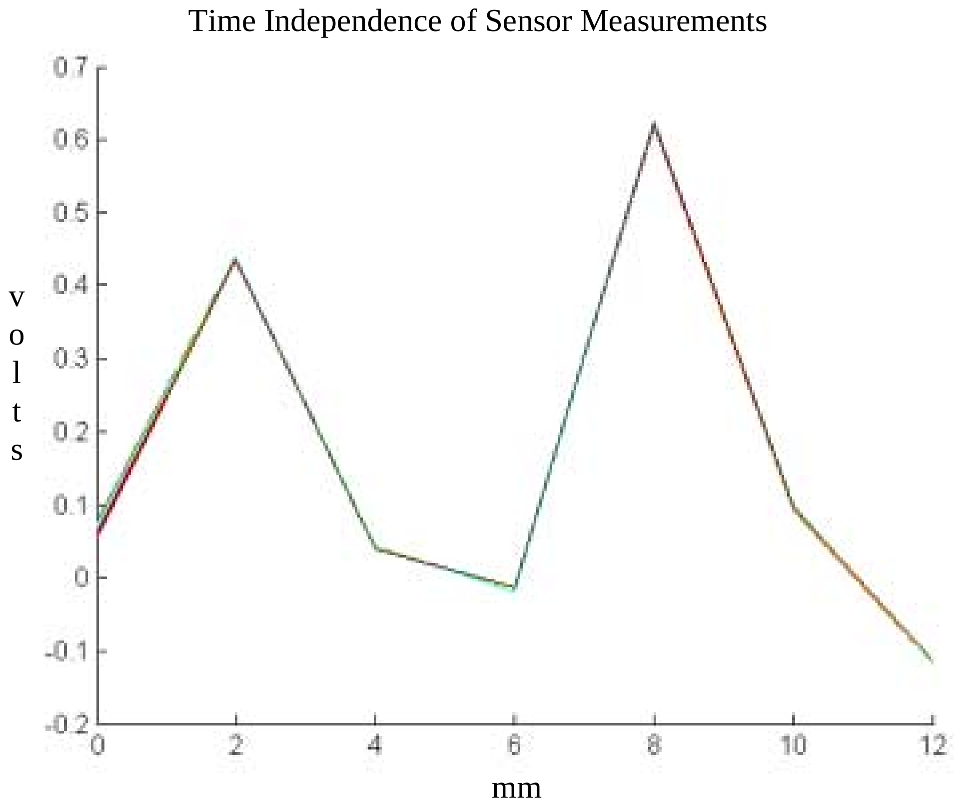

Figure 3-6. Response of one row of the pressure sensor's elements after 10 trials.

3.3.2 Manual Positioning Error

It is important to know whether the pressure sensor measurements are repeatable, and so in order to study this we laid the sensor flat and a stationary object was laid stationary on top of the sensor. Data was read from each element of the sensor. The object was then removed for one minute and then placed back on the sensor at approximately the same location, and data was again read from each element of the sensor. This process was repeated ten times, and the various measurements from the sensor were compared to determine if they were repeatable. We repeated the entire process using two different object curvatures and two different masses for each curvature.

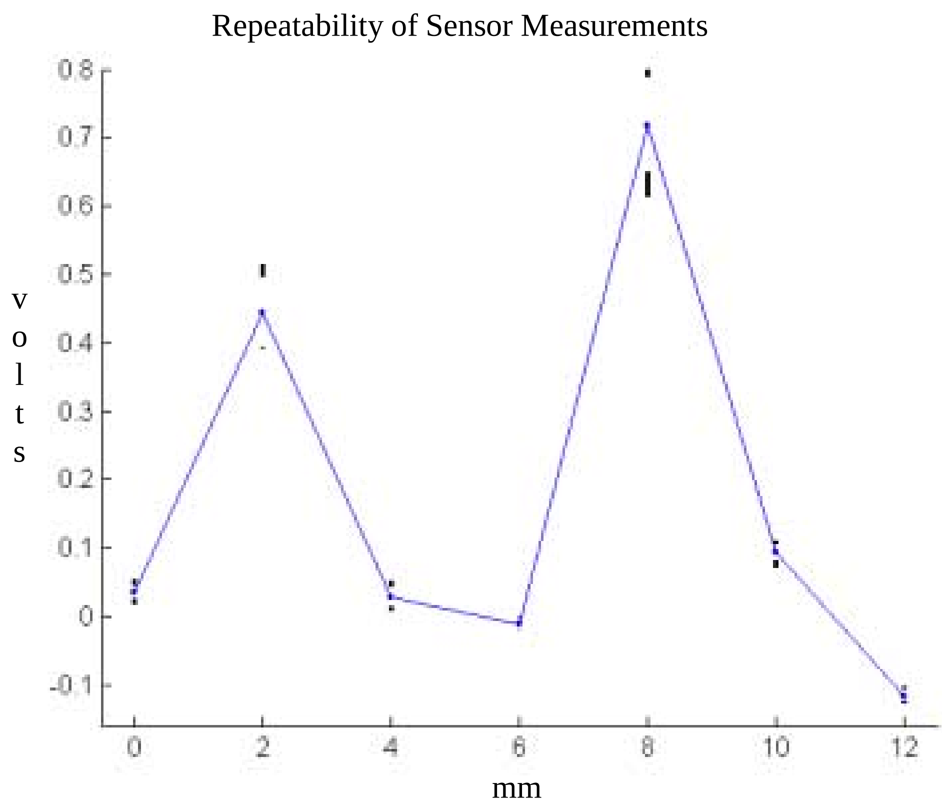

Figure 3-7. Response on sensor to repeated measurement of object placed and then removed from one row of sensor elements. The thin line joins mean measurements at different elements. At each point the black bars indicate the maximum and minimum measurement. The space between the bars and the mean is one standard deviation.

Figure 3-7 shows the response of one row of sensor elements; with the line representing the average reading. The average standard deviation of the seven elements in the row was 0.02458 or 26.4% of the measurement; with an average range of 0.0686 volts. The large error present in the result is due to the object not being placed in exactly the same location when the object was removed and then replaced. The object that was applied to the sensor and the position it was applied are shown in Figure 3-5. The response of the sensor indicates that manual positioning errors can be a significant source of experimental error. Accordingly, we elected to rigidly stabilize the back of the fingerpad in our experiments, and to apply the sensor with a motorized positioning stage with fine spatial precision.

3.3.3 Linearity in Response to Pressure

To further understand the characteristics of the pressure sensor, we designed a method to apply a known force along the sensor elements and record the data. The setup consisted of the motion platform, a flat plate to attach the sensor, an Aurora Scientific Model 300B Dual Mode Lever Arm System, and a stand to hold the Aurora System. The motion platform was used to move the sensor in the *x* and *y* direction by finite distances, and the Aurora Lever Arm System was used to apply a known force to another object with cylindrical indenting tips of various sizes. Several different sized tips were carefully manufactured from brass into a cylindrical shape with a very flat base in order to apply a uniform load. The diameters of the cylindrical tips that were made were 0.4mm, 0.5mm, 0.8mm, 1.2mm, 1.6mm, and 1.7mm.

We tested the sensor to determine if its measurements were linear. In order to accomplish this, we applied various forces to the sensor element with the 0.5mm diameter Aurora tip. We applied five forces to ten points along the x axis of sensor element 0x54. These forces were 0.01N, 0.02N, 0.03N, 0.04N, 0.05N, 0.06N, 0.07N, 0.08N, and 0.09N. Figure 3-8 shows a plot of the sensor response from the various forces. Figure 3-9 shows the response at the peak of the element which occurs approximately at 1.5mm point of Figure 3-8. A linear fit to the data had a slope of 0.1726 volt/gram, a bias of –0.1830 volt, and a R^2 value of 0.9778. Figure 3-10 shows the response of the element at the 1.0mm point of Figure 3-8. A linear fit to these measurements had a slope of 0.1269 volt/gram, a bias of –0.1008 volt, and a R^2 value of 0.9846. In both cases, the sensor output with increasing force was slightly sigmoidal. Over the force ranges shown in Figures3-9 and 3-10 deviation from linearity was found to be 6.5% to 7.1% of the maximum reading.

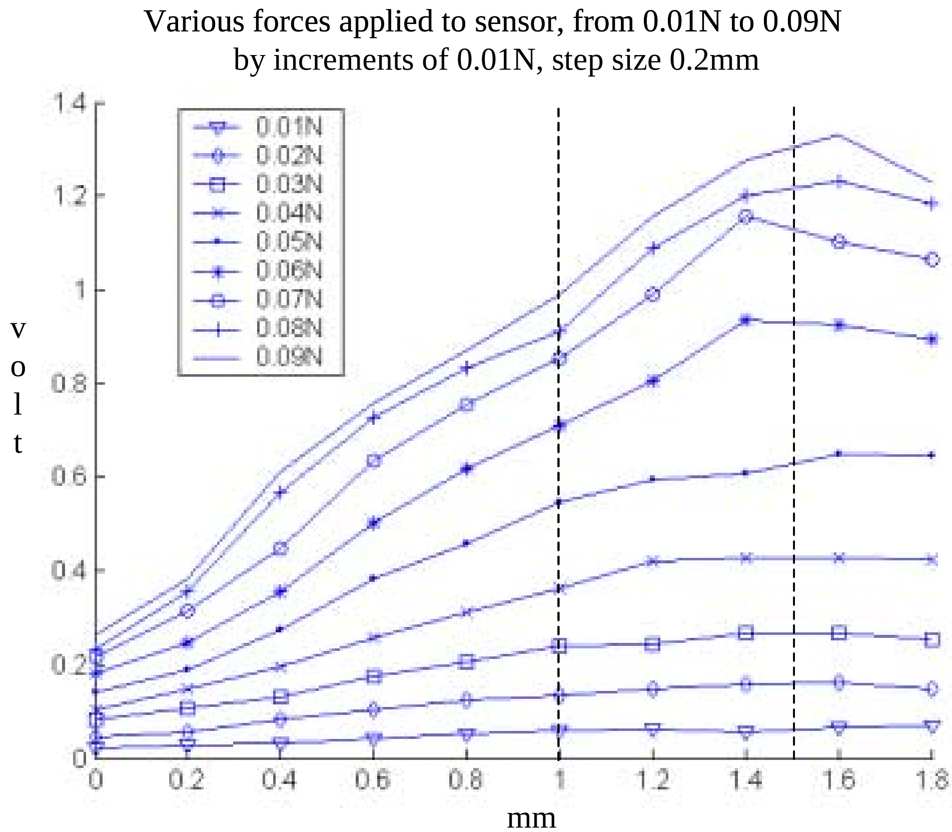

Figure 3-8. Various forces of 0.01N to 0.09N were applied to element 0x54 with a 0.5mm diameter cylindrical tip.

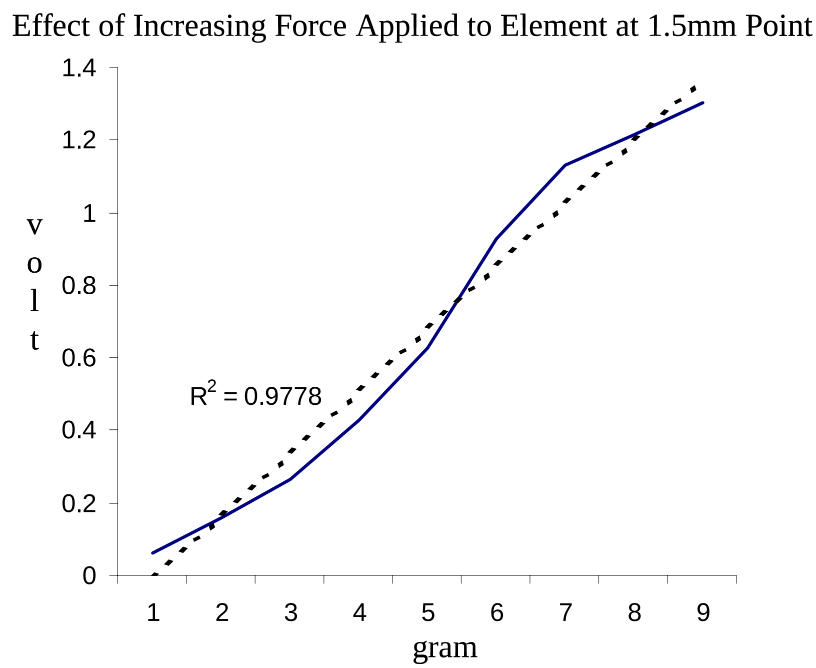

Figure 3-9. Various force levels applied to 1.5mm point of the sensor element 0x54.

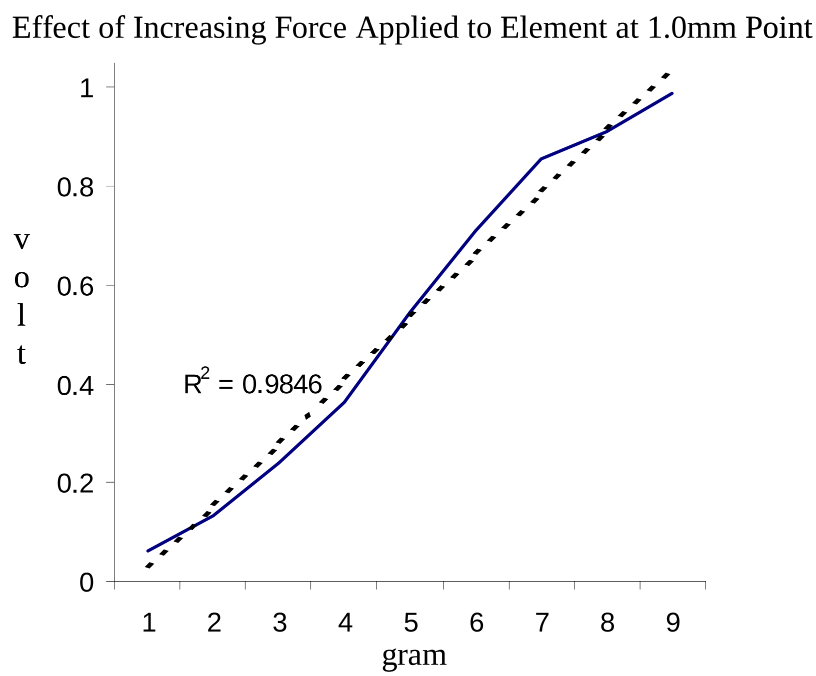

Figure 3-10. Various force levels applied to 1.0mm point of the sensor element 0x54.

We also tested the sensor to see if applying different sized indentor tips to an element with the same force would cause an appropriate element scale response. We applied the same force using the Aurora 0.4mm, 0.8mm, 1.2mm, and 1.6mm tips to element 0x54, and we found that the peak values were somewhat linear, as the tip size changed. Figure 3-11 shows the result.

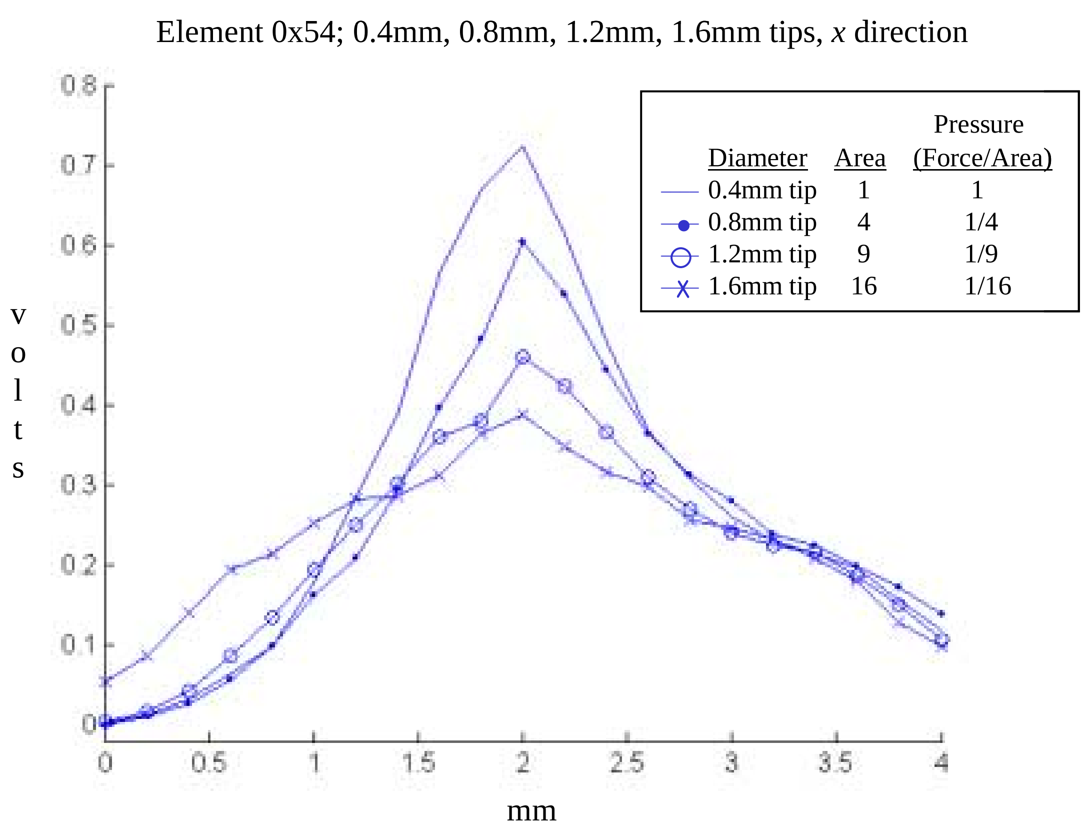

Figure 3-11. The same force applied to element 0x54 along the positive *x* direction using the Aurora 0.4mm, 0.8mm, 1.2mm, and 1.6mm tips.

3.3.4 Anisotropy

The response profile of the sensor was different when the indentor was stepped in the *x* direction than in the *y* direction. To explain this anisotropy, we attached the sensor to the flat plate with double sided tape in the orientation shown in Figure 3-12. We applied a force of 0.075N with the 0.5mm Aurora tip to element 0x56 and stepped along the *x* direction. We then returned to the center of element 0x56 and applied a force of 0.075N while stepping along the *y* direction. Figure 3-13 shows both of these results. The response of the element has a narrower distribution when the indentor is applied along the *x* direction, and the response in the y direction is broader.

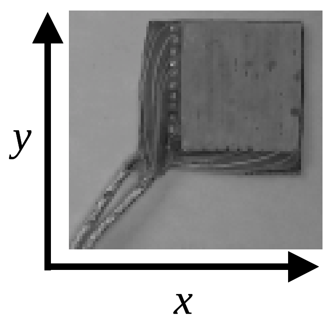

Figure 3-12. Pressure sensor with the orientation of the positive x direction and positive y direction specified.

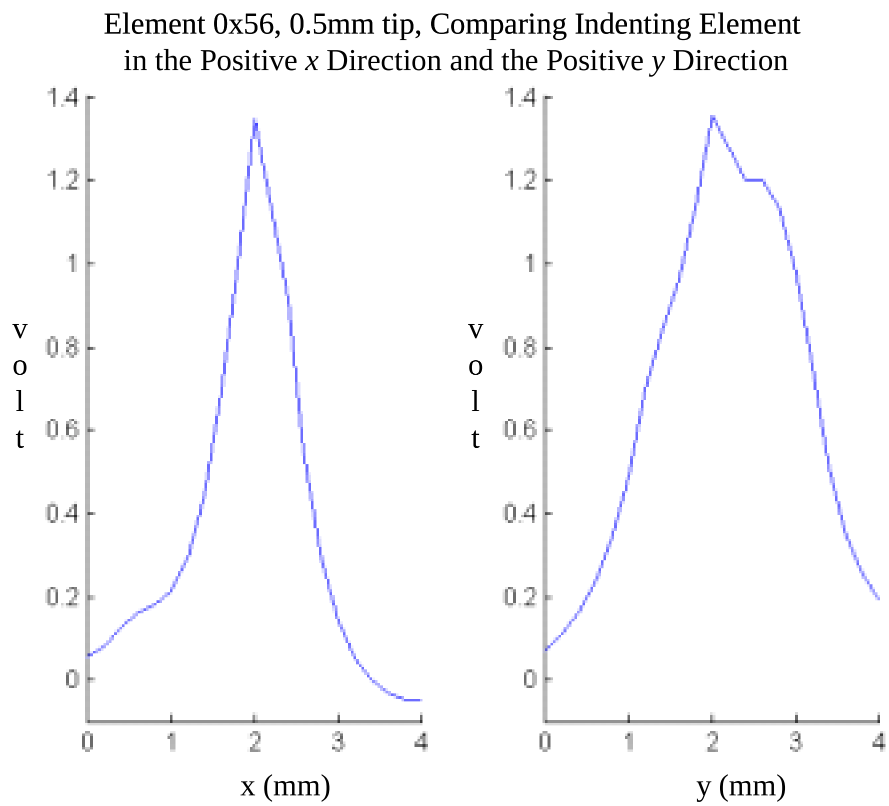

Figure 3-13. Aurora tip with 0.5mm diameter translated along the positive *x* and *y* direction of element 0x56. The response of the element has a narrower distribution when the indentor is applied along the *x* direction than in the *y* direction.

This results implies that the direction in which measurements are read from the sensor is important. To further confirm the anisotropy we rotated the orientation of the sensor on the flat plate 90 degrees, as shown in figure 3-14. We then repeated the previous test by applying a force along the *x* direction, returned to the center of element 0x56, and then applying a force along the *y* direction. Figure 3-15 show both of these results. From these results, we can conclude that the orientation of the sensor when taking measurements does matter.

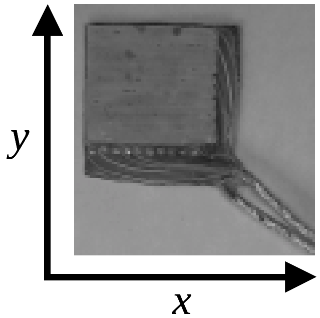

Figure 3-14. Pressure sensor rotated 90° degrees with the orientation of the new positive *x* direction and new positive *y* direction specified.

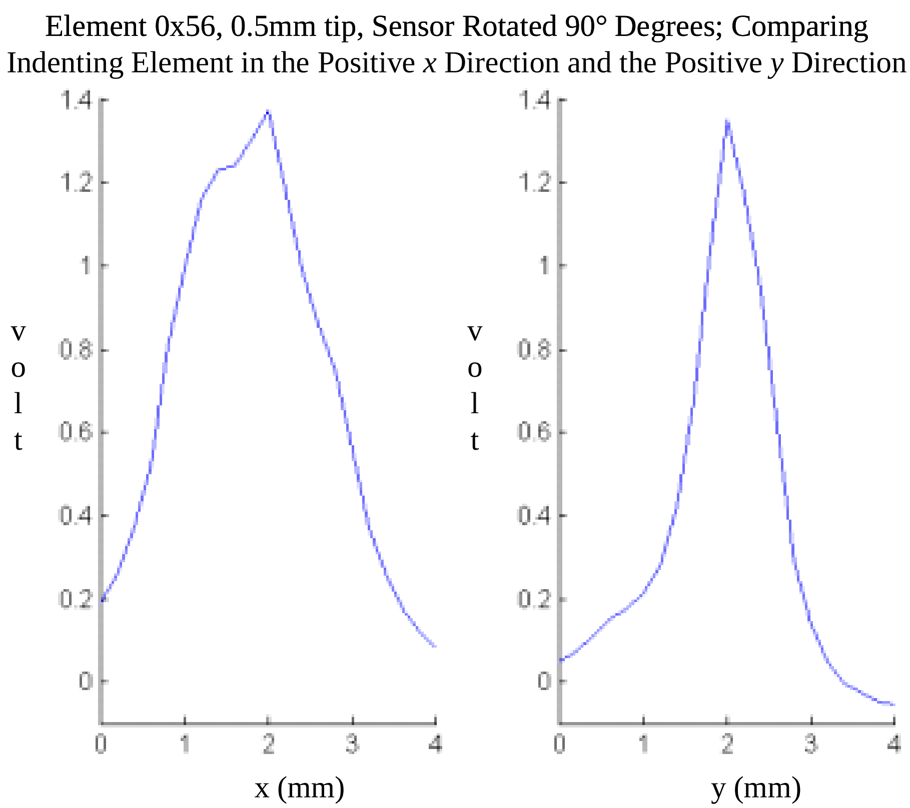

Figure 3-15. Aurora tip with 0.5mm diameter translated along the new positive *x* and *y* direction of element 0x56.

3.3.5 Inter-Element Variability

We next studied the similarities and differences between different elements. We tested the sensor to see if other elements exhibited a narrower response in the *x* direction than the y direction. We did this by applying the same amount of force from the 0.5mm Aurora tip across elements 0x54 and 0x56. We first applied a force of 0.075N to each element and stepped along the x direction, and then returned to the center of each element and applied the same force while stepping along the y direction. Figure 3-16 show the results of a) element 0x54 and b) element 0x56. The response along the x direction was narrower than the response in the y direction for both elements.

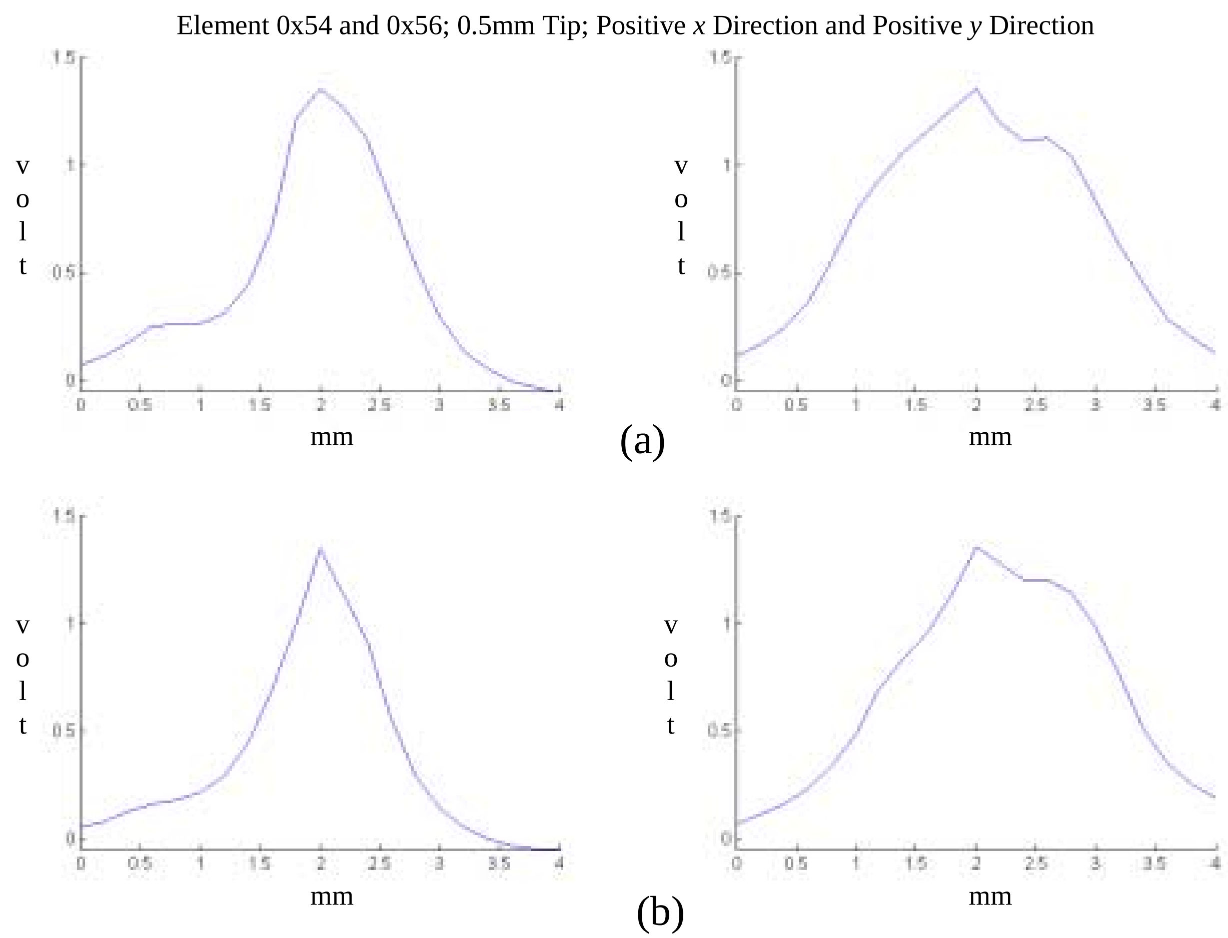

Figure 3-16. The same 0.075N force from the 0.5mm Aurora tip was applied in the positive x and y direction for a) element 0x54 and b) element 0x56.

We also tested various elements to determine if their peak values and response were the same, so we applied the same 0.075N force using the Aurora 0.4mm, 0.8mm, 1.2mm, and 1.6mm tips to four different elements. The elements we used were elements 0x52, 0x54, 0x63, 0x65. Figure 3-17 shows the results from the four elements. We found that all four elements had a similarly shaped response. However, the peak value of each element was different. Elements 0x52 and 0x65 had similar peak values, while elements 0x63 and 0x54 had similar peak values. No two elements had the exact same peak value even though the same force was applied to each sensor.

Elements 0x52, 0x54, 0x63, 0x65; Used 0.4mm, 0.8mm, 1.2mm, 1.6mm Aurora Tips

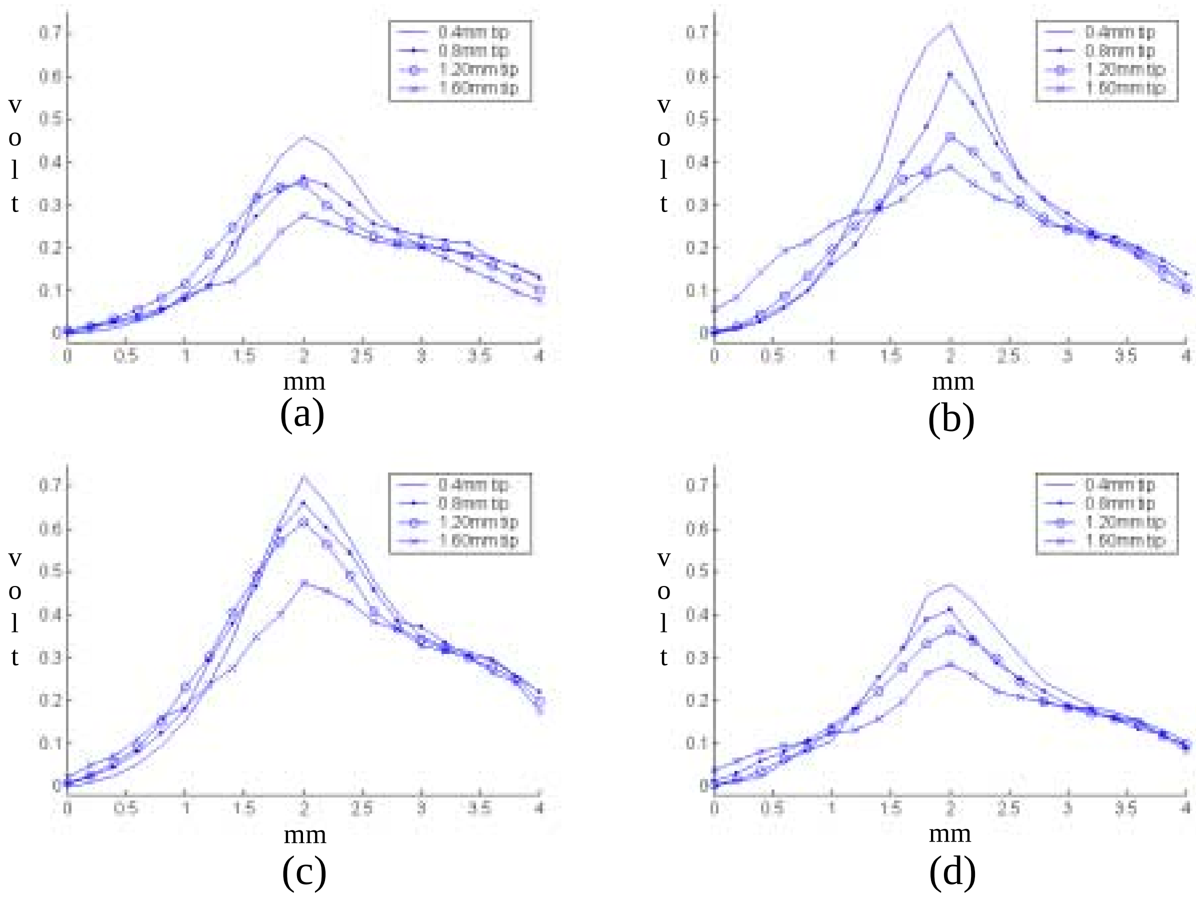

Figure 3-17. A force of 0.075N force using the Aurora 0.4mm, 0.8mm, 1.2mm, and 1.6mm tips were applied to elements a) 0x52, b) 0x54, c) 0x63, and d) 0x65.

3.3.6 Spatial Response Profile

We were interested in measuring the response of an element to a line load, because the spatial response profile would aid us in using signal processing techniques to increase the spatial resolution of pressure measurements. In order to measure the spatial response profile we placed the sensor around the 1 inch diameter cylinder. We slightly dulled a razor blade to protect the sensor, and then placed it in a vice to hold it parallel to the sensor. The width of the razor edge was measured to be 0.0023 inches using a Nikon Measurescope. Figure 3-18 shows the experimental setup. Data from only element 0x54 was accessed during this experiment.

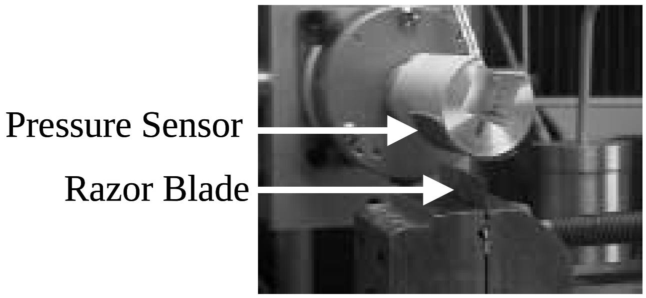

Figure 3-18. The experimental setup used to measure the spatial response profile of element 0x54 of the pressure sensor. A dulled razor blade is used to indent the sensor while it is wrapped around a 1 inch diameter cylinder.

We applied the load of the sensor to the razor blade, with a small amount of force. Then we raised the sensor and moved it in the *x* direction by a distance of 0.033mm, and again applied the load to the razor blade. We repeated this process until we translated the razor across the one element, and then repeated this entire process twice. The first time we applied a load of 1.0 grams to the razor blade, and the second time we applied a load of 2.3 grams to the razor blade. Figure 3-19 shows the results of applying the line load to the sensor both times.

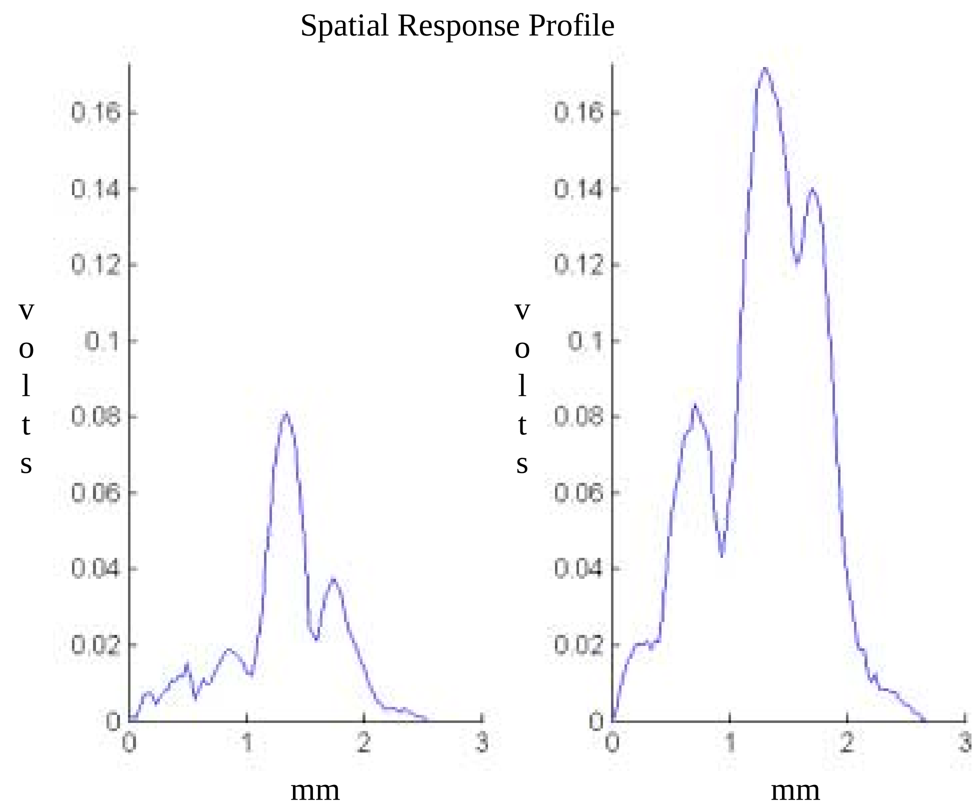

Figure 3-19. Spatial response profile produced by a razor blade indenting the sensor element 0x54 with a load of 8.8 grams and 18.7 grams, respectively

3.3.7 Sensor Resolution

The size of each element of the sensor is 2mm by 2mm, so we wanted to determine the smallest possible spatial resolution of the sensor response. We accomplished this by having a pattern of lines micro-machined on a silicon wafer and then measured the sensor response to this pattern. Figure 3-20 shows the pattern we micro-machined onto a silicon wafer using photolithography. The height of each line is 0.100mm and the thickness of each line is 0.02116mm.

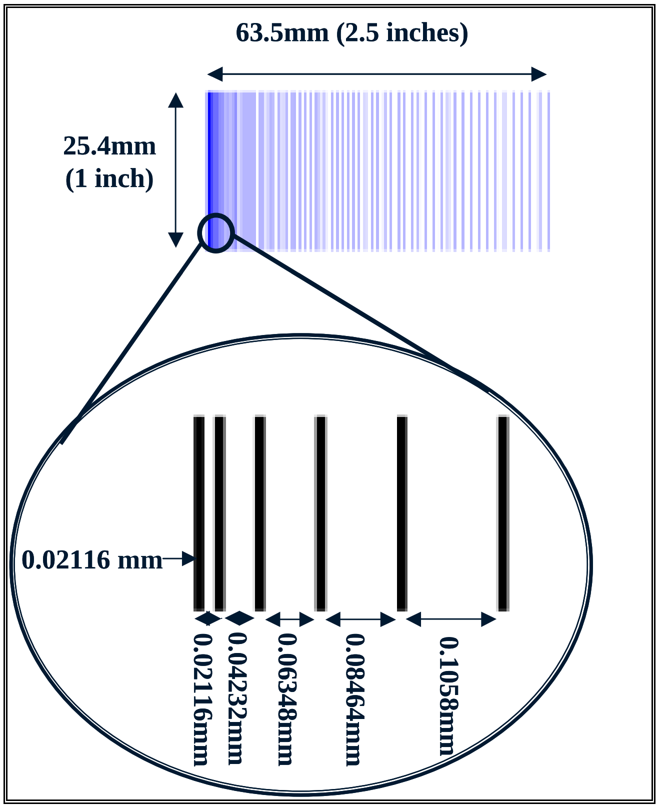

Figure 3-20. Pattern micro-machined onto a silicon wafer using photolithography. The height of each line is 0.100mm and the thickness of each line is 0.02116mm.

In order to measure the response of the sensor to the silicon wafer, we first placed the sensor around the 1 inch diameter cylinder, and then applied the sensor to the wafer with a small amount of force, read data from one sensor element, removed the sensor from the wafer, and then moved the sensor by a finite distance along the x direction of the wafer. We repeated this process until we translated it across the entire wafer (Fig. 3-21). The resolution of the sensor can then be determined by measuring where the spatial frequency response becomes apparent. We used the Raleigh's criterion to justify the finest resolution possible for the sensor. The spatial resolution based on Raleigh's criterion is 0.75mm.

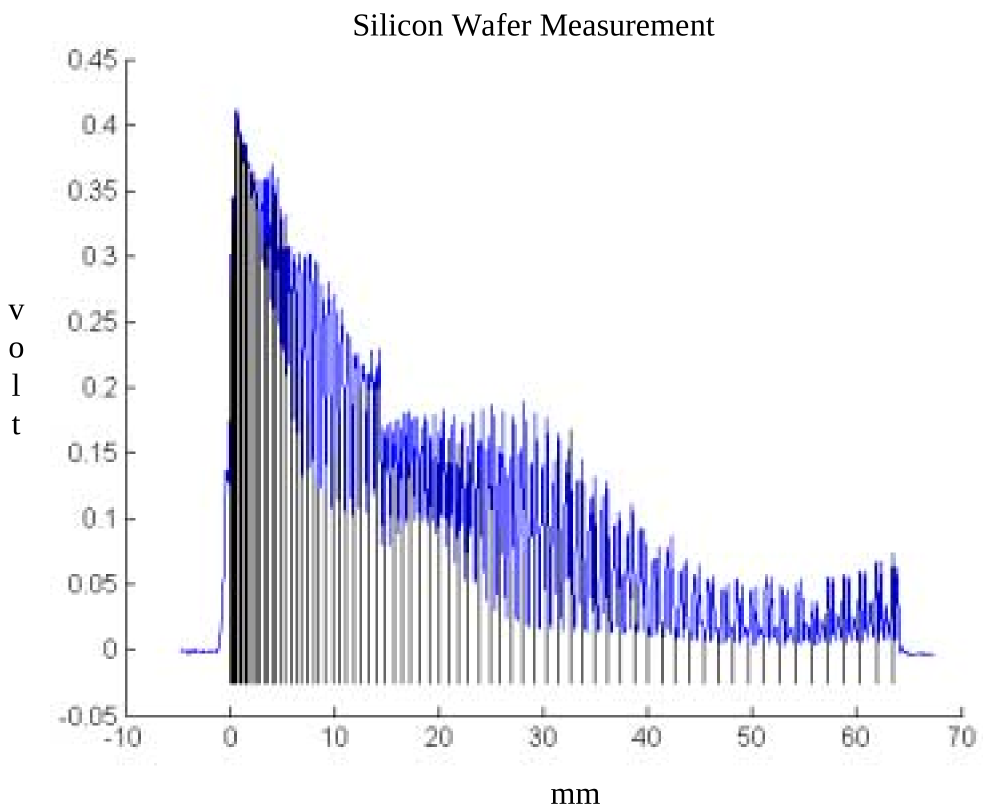

Figure 3-21. Response of the sensor to being translated across the silicon wafer.

3.4 Pressure Sensor Calibration

The output of the pressure sensor to the PC is in volts, and so in order to convert the pressure sensor output of voltage to pressure, we needed to calibrate the sensor. To do this we applied a uniform pressure over the surface of each element using water pressure, placing the sensor on a flat surface and a waterproof bag on top of the sensor. The bag was filled with water to various heights ranging from 3.6 inches to 7.6 inches and readings were taken from all elements of the pressure sensor.

The pressure was then calculated from the height of the water using the equation, $\Delta p = \rho g h$, where ρ is the density of water, g is gravity, and h is the height of the water in the bag. Figure 3-22 shows the pressure from all elements. The voltage from each element can be converted to pressure by fitting a line to the data and using it as a voltage to pressure conversion table. Figure 3-23 shows the data from element 0x54. A linear line was fit to the data and found to have a slope of 0.00002652 volt/gram, and a R^2 value of 0.9618.

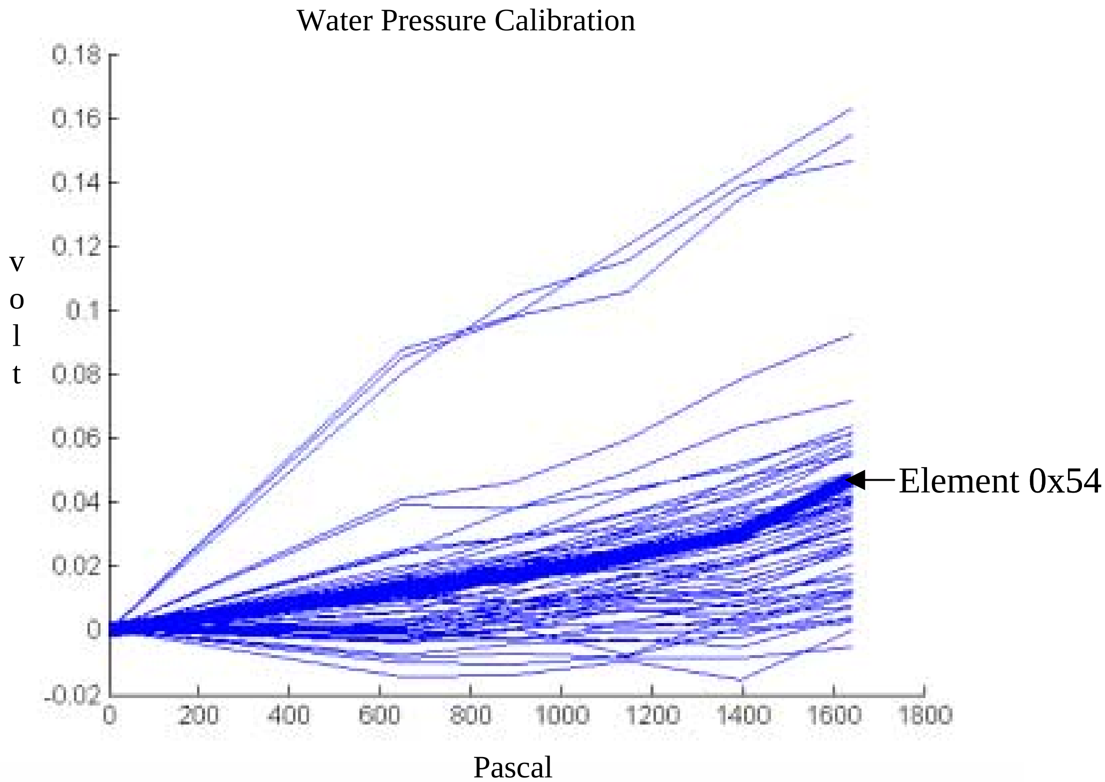

Figure 3-22. Various levels of water pressure applied to all elements of the sensor in order to convert from sensor voltage to pressure.

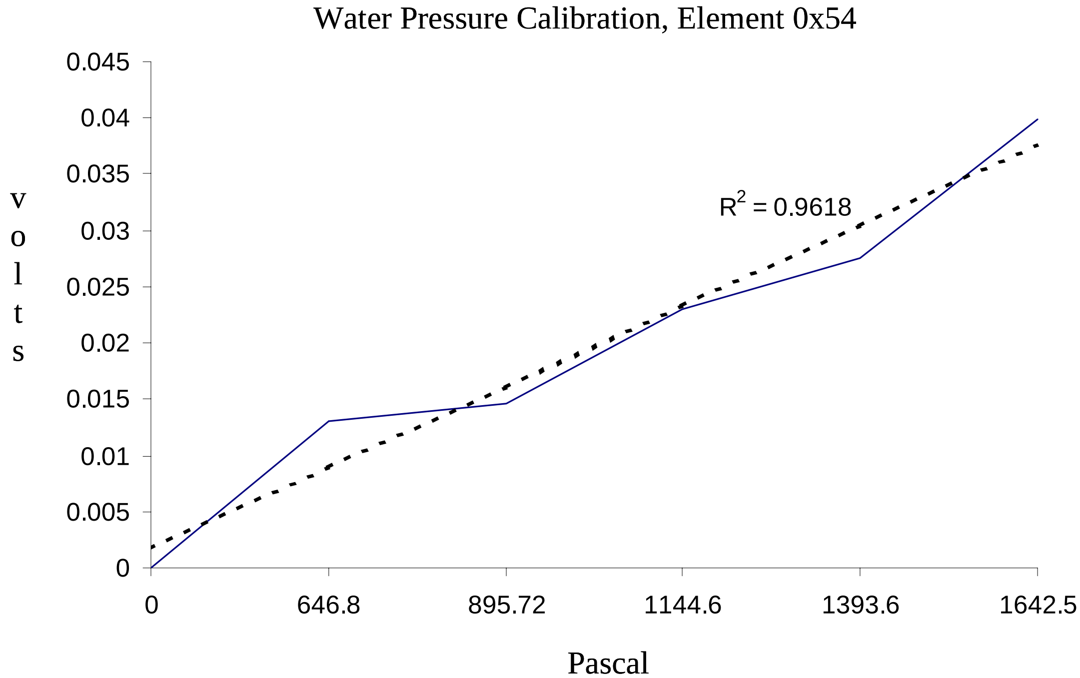

Figure 3-23. Water calibration of element 0x54. A linear fit to the data had a slope of 0.00002652 Volt/Pascal, and a R^2 value of 0.9618.

3.5 Linearity in Terms of Spatial Summation

The response of a sensor element to a line load was measured in Section 3.3.6, and the response of each element of the sensor to a uniform load was measured in Section 3.4. We then wanted to determine whether the sensor elements exhibit linearity in terms of spatial summation. The summation of the pressure measured by the sensor from the line load across element 0x54 should be equal to the pressure measured by applying a uniform load to the element. Figure 3-24 illustrates this question of whether the response of the sensor to uniform water pressure over the entire element is equal to the summation of the response of the sensor to a line load across the element.

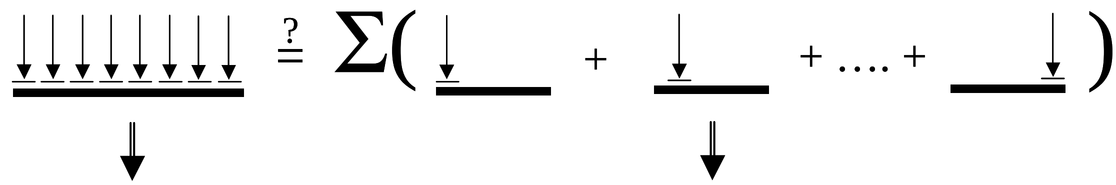

$$V_{\text{Water Pressure}} \stackrel{?}{=} \sum\left(V_{\text{Line Load 1}} + V_{\text{Line Load 2}} + \ldots + V_{\text{Line Load n}}\right)$$

Figure 3-24. Illustration of whether the response of the pressure sensor to uniform water pressure is equal to the summation of the response of the sensor to a line load. The uniform water pressure over one sensor element is illustrated on left side of the equal sign. The summation of the response from a line load translated across one sensor element is illustrated on the right of the equal sign.

The summation of the line load across element 0x54 was found to equal 5.2254 volts, while under the same load the voltage from a uniform load was found to equal 4.5482 volts. This result indicates that the pressure sensor exhibits approximate linearity in terms of spatial summation, since the two summations differ by roughly 13%. This difference may have been within experimental error of the water pressure calibration method, or may have been due to nonlinearity in spatial summation by the sensor. Repeated calibration using water pressure would be required to put an upper bound on the contribution of this calibration method to the observed 13% difference.

3.6 Prospects for Deconvolution

Simulation suggests that deconvolution may increase the spatial resolution of the pressure measurements. Figure 3-25 shows simulated, noise-free pressure data before (left) and after (right) deconvolution. The deconvolved pressure distribution shows an increased resolution of finger ridges and grooves. However, in order for deconvolution to improve the spatial resolution of pressure measurements, the pressure sensor must produce linear measurements and be shift-invariant.

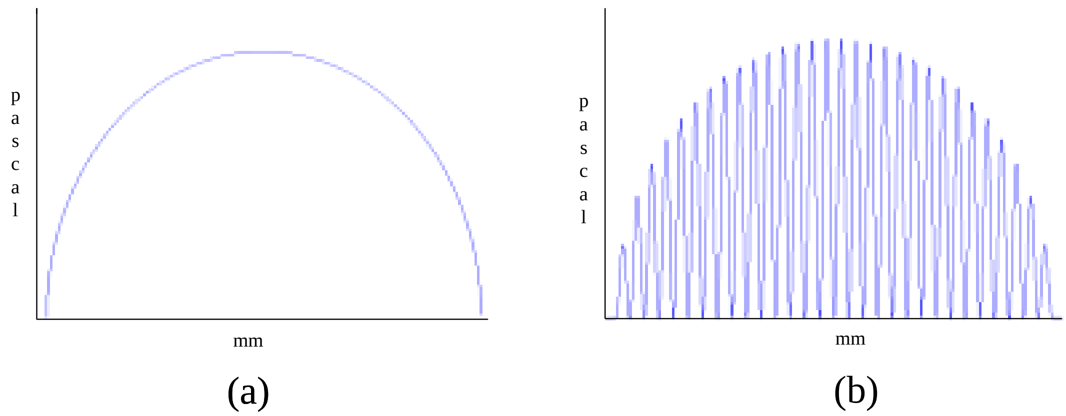

Figure 3-25. Schematic illustrating the pressure distribution measurements a) before the use of deconvolution and b) after the use of deconvolution. The use of deconvolution will increase the spatial resolution of the measurements in order to see finger ridges and grooves more clearly.

Based on the properties of the sensor measured in section 3.3, deconvolution is not ruled out. However, we observed many sources of noise that might limit the success of this technique. Sensor noise gave repeated measurements of the same load a standard deviation of 4.5%. When forces of 0.1-0.9 N were applied to two indentors with different diameters, nonlinearity in response to the increasing forces lead to errors in pressure that were 0 to 7.1% of the voltage observed at 0.9N. Nonlinearity in terms of spatial summation was shown to distort the measurement by less than 13%, but the lower bound remains unknown. Finally, the spatial response profile (Figure 3-19) of the sensor had several peaks. These observations suggest that deconvolution -- which is sensitive to all of these sources of error – may be difficult.

3.7 Summary

In this chapter we established to what extent sensor measurements were repeatable, linear, and anisotorpic. Gain for each element of the sensor was found to vary significantly. The spatial response profile was measured and the sensor was measured using a line load. A uniform load under water pressure was used to find a factor for converting sensor voltages to pressures. Due to the anisotropy of the sensor, we chose to shift the sensor in the x-direction exclusively. We also examined the use of deconvolution to increase the spatial resolution of pressure measurements, but found that due to sensor noise content and the complexity of the spatial response profile the success of deconvolution may be limited.

4.0 Finger Pad Pressure Measurement

4.1 Methods

We measured the pressure distribution on the index finger pads of five subjects, as two rigid indentors were used to load the pad at forces ranging from 25 to 175 gramf. The indentors were cylindrical, with diameters of 1 and ½ inch. The pressure sensor array, which was situated between the indentor and skin, was used to sample interfacial pressure at different points in the contact area. Figure 4-1 shows orientation of the finger and cylinder, and our convention for displaying the interfacial pressure in subsequent figures.

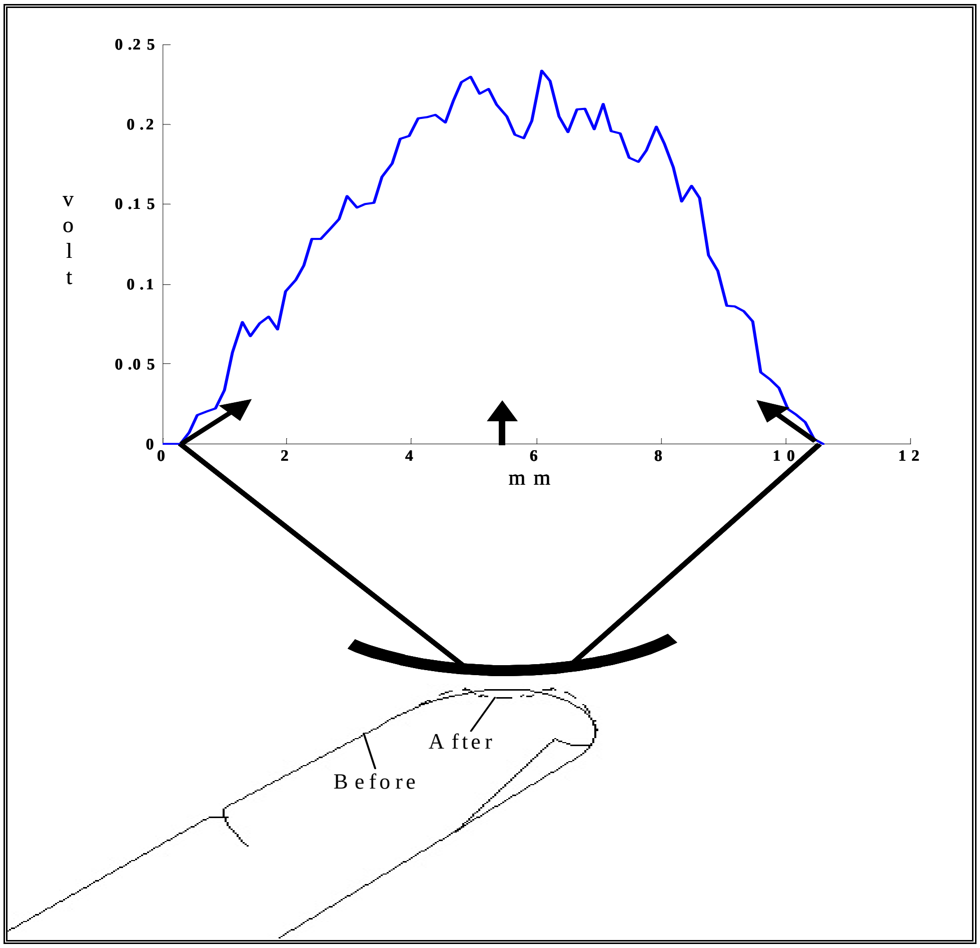

Figure 4-1. Illustration of the measurement of the pressure distribution from the finger pad using a curved indentor. The deformation of the finger before and after a load is applied are marked. The arrows indicate the force or pressure components measured.

During the experiment we measured voltage on one element (0x54) of the pressure sensor. At the start of each measurement, we used the motion platform to rotate the indentor and pressure sensor to a known position on the fingertip and then applied a known net force. Between measurements, the motion platform raised the indentor off the fingertip, and then rotated it by a known arc length. The sensor was then returned to the fingertip with the same net force, and another pressure measurement was taken. This process was repeated until the sensor element had rotated entirely across the fingertip. All measurements were saved in a PC data file. Figure 4-2 illustrates the process. To obtain fine spatial resolution the shifts in sensor location were far smaller than the 2mm sensor element width. In a typical experiment, 100 measurements were taken over a 10mm arc. To minimize the effect of drift in the sensor, the data just before contact was used as a baseline for pressure measurements.

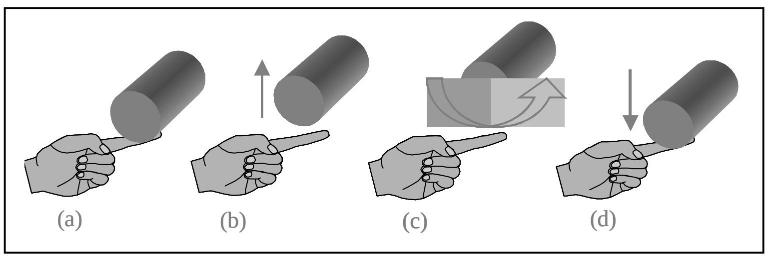

Figure 4-2. The process used to measure the pressure distribution of the finger pad. The pressure sensor is situated between the object and finger pad. The finger pad (a) is indented with the cylindrical object, (b) the object is removed from the finger pad, (c) the object is rotated by a known amount, and then (d) the object again indents the finger pad. This process is repeated until the pressure sensor measures the entire contact area of the finger pad.

4.2 Results

We applied various net forces with two different cylindrical indentors to the finger pads of five subjects. Our results show the effect of changes in net force and indentor curvature on the magnitude and shape of the pressure distribution. Asymmetry in the pressure distributions was expected, since the resting curvature of the fingerpad surface varied from the proximal to distal edge of the contact area.

4.2.1 Intra-Subject Variability

We first consider the effect of indenting the finger pad of various subjects with the same sized cylinder. Figure 4-3 compares the results of applying a 50 gram net force with a 1 inch diameter cylinder to the finger pad of subjects 1 and 2. The resulting magnitude and shape of the surface tractions are very similar for both subjects.

Subject 1 and 2: 1 inch Diameter Cylinder, ~50g Net Force

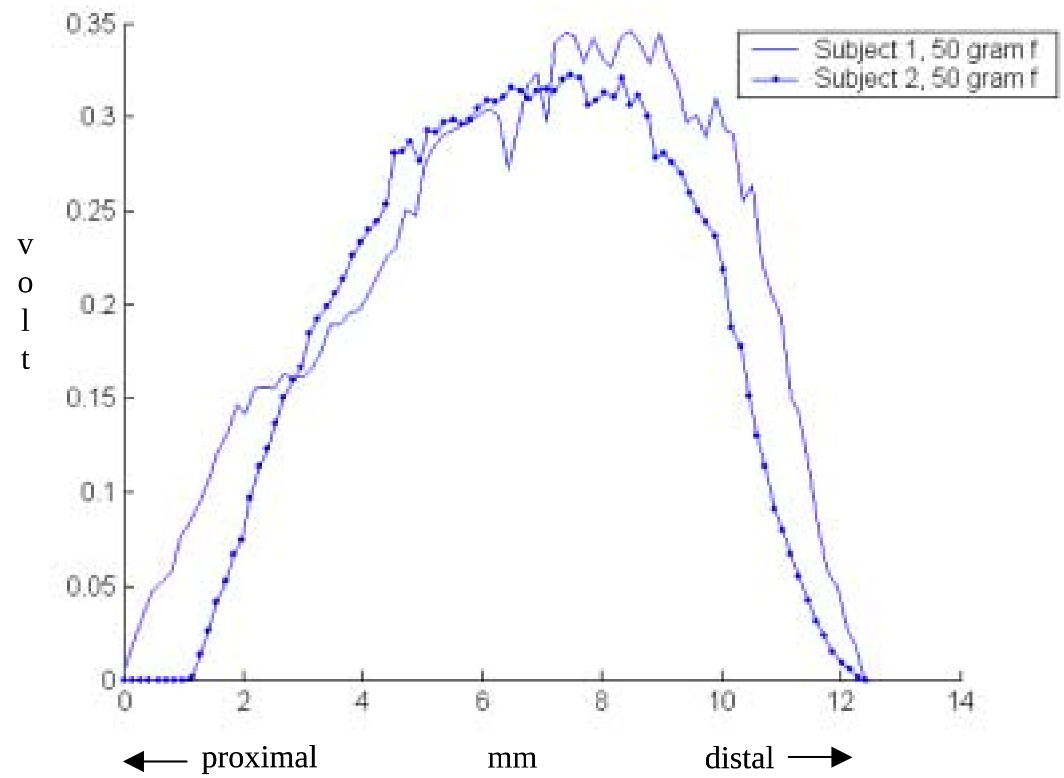

Figure 4-3. Pressure distribution measurement of subject 1 and subject 2. Both subjects were indented with net force of 50 grams using a 1 inch diameter cylinder.

Figure 4-4 compares the results of applying approximately a 25 gram net force with the ½ inch diameter cylinder to the finger pad of subjects 2, 3 and 4. The shape of the surface tractions are very similar for all three subjects. The peak values of the surface tractions vary between the subjects by about 50%. This difference may in part reflect noise in the load cell sensing net force, since 25 gramf is in bottom 2.5% of the operating range of the device.

Subject 2, 3, and 4: 1/2 inch Diameter Cylinder, ~25g Net Force

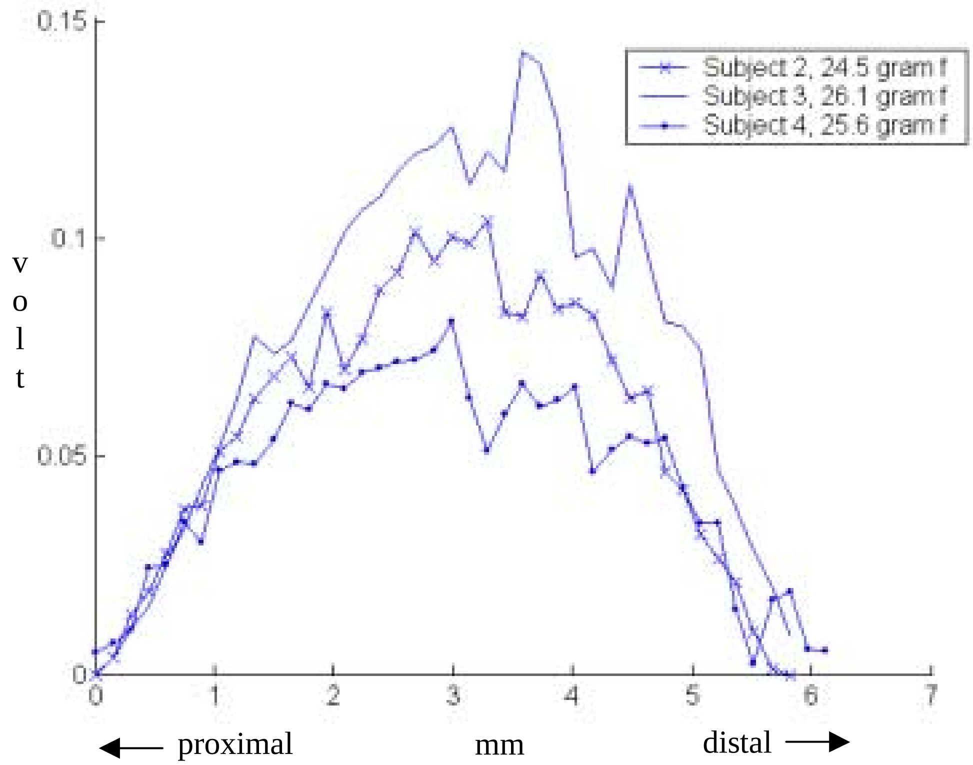

Figure 4-4. Pressure distribution measurement of subjects 2, 3, and 4. All three subjects were indented with a net force of approximately 25 grams using a ½ inch diameter cylinder.

4.2.2 Effect of Varying Radius

Figure 4-5 compares the results of applying a net force of approximately 50 grams with both the 1 inch and ½ inch diameter cylinder to the finger pad of subject 5. Both surface tractions have an approximately trapezoidal distribution. As expected, the peak magnitude of the surface traction under the ½ inch diameter cylinder is greater than the peak magnitude under the 1 inch diameter cylinder. Accordingly, the lower peak pressure under the 1 inch diameter indentor is compensated by the greater width.

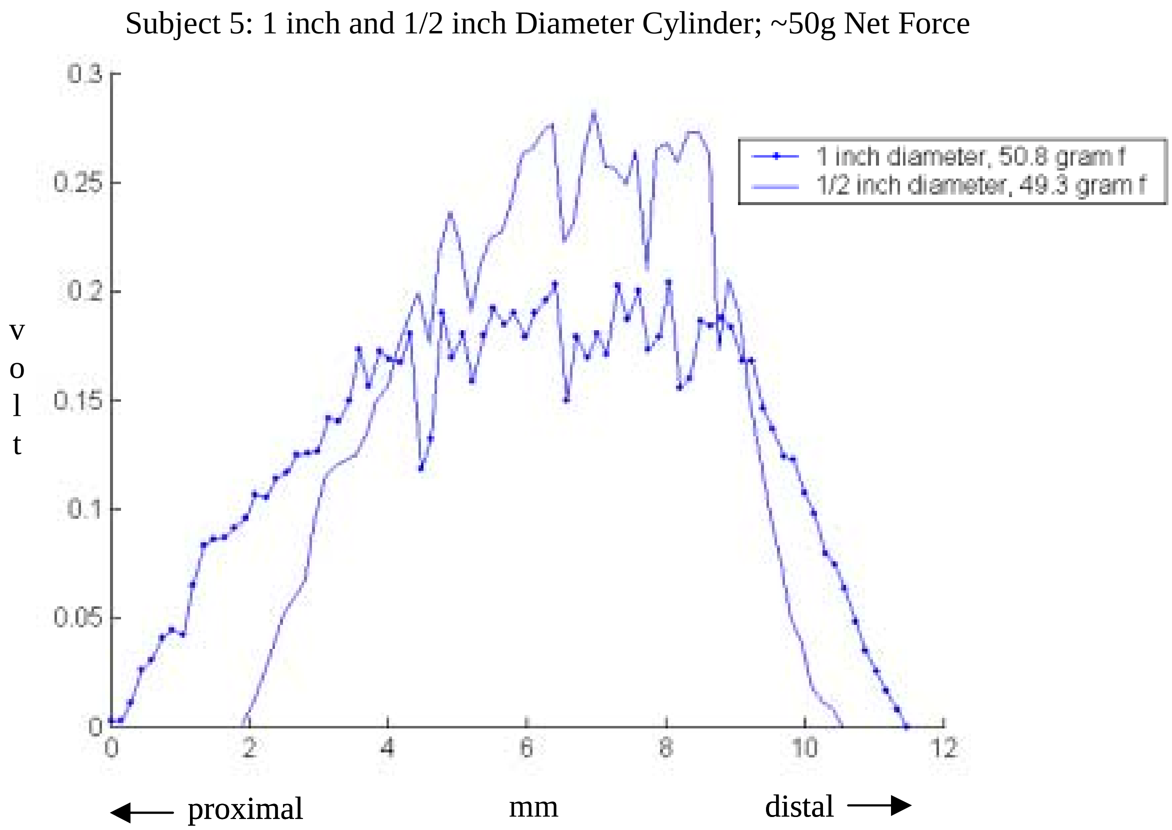

Figure 4-5. Pressure distribution measurement of subject 5 using a 1 inch diameter cylinder with a net force of 50.8 grams compared to the pressure distribution measurement of subject 5 using a ½ inch diameter cylinder with a net force of 49.3 grams.

Figure 4-6 shows the combined effects of intersubject variability and change in surface curvature. The results of applying a 52.2 gram net force with the 1 inch diameter cylinder to the finger pad of subject 2 and applying a 56.1 gram net force with the ½ inch diameter cylinder to the finger pad of subject 3 are presented. The magnitude of the resulting surface traction from the ½ inch diameter cylinder is again greater than the magnitude from the 1 inch diameter cylinder, and the overall shape of both resulting surface tractions are similar. Again, the width of the surface traction from the 1 inch diameter is wider than the width produced by the ½ inch diameter cylinder.

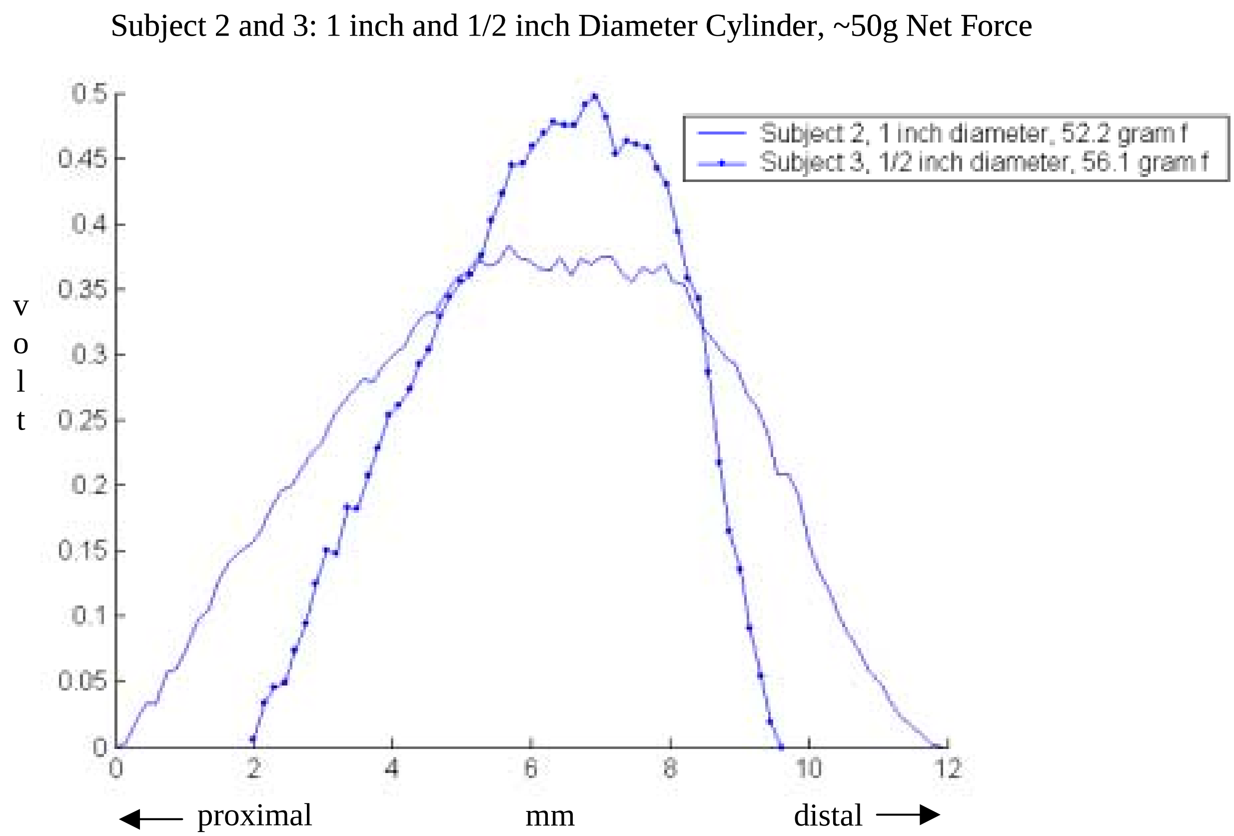

Figure 4-6. Pressure distribution measurement of subject 2 using a 1 inch diameter cylinder with a net force of 52.2 grams compared to the pressure distribution measurement of subject 3 using a ½ inch diameter cylinder with a net force of 56.1 grams.

4.2.3 Varying Net Force

We varied the net force that was applied to the finger pad of the subjects while using the same sized cylindrical indentor. Figure 4-7 shows the results of applying a net force of 22.6 grams, 52.2 grams and 106.1 grams to the finger pad of subject 2 with the same 1 inch diameter cylindrical indentor. The general shape of the pressure distribution for all three force levels is similar, with the magnitude of the pressure distribution increasing as the net force level increases. The width of the surface traction also increases as the net force increases, though this effect appears to saturate between 50 and 100 gramf.

Subject 2: 1 inch Diameter Cylinder, 22.6g, 52.2g, and 106.1g Net Force

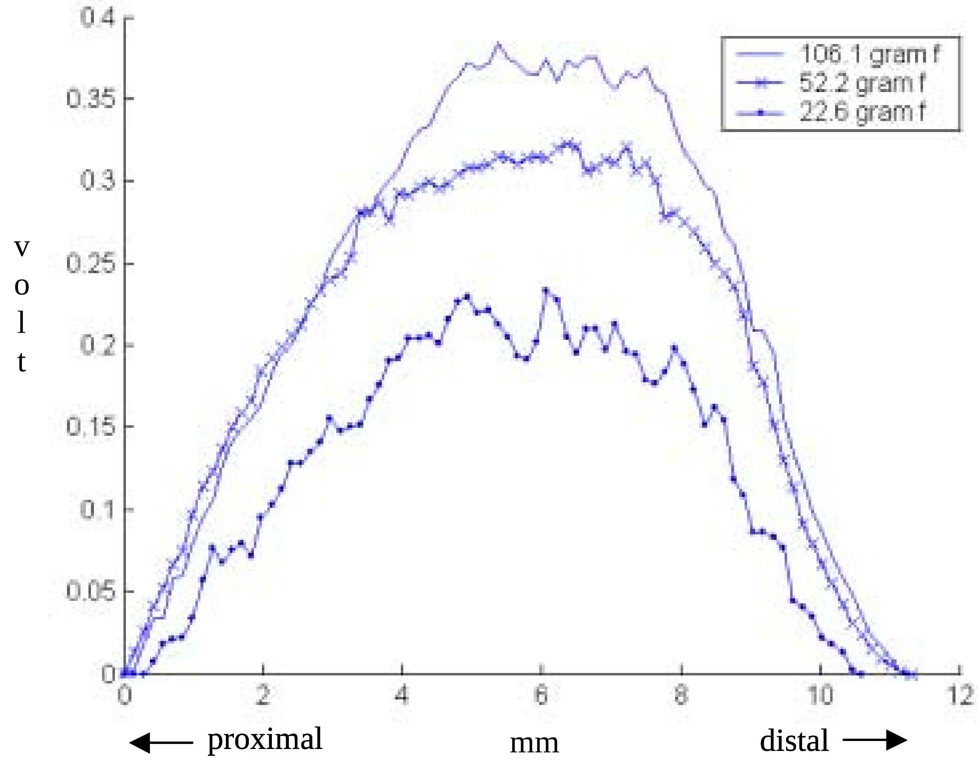

Figure 4-7. Pressure distribution measurement of subject 2 using a 1 inch diameter cylinder with a net force of 22.6 grams, 52.2 grams, and 106.1 grams.

Figure 4-8 shows the results of applying a net force of approximately 50 grams, 75 grams and 175 grams to the finger pad of subject 1 with the same 1 inch diameter cylindrical indentor. Once again, the general shape of the pressure distribution for all three force levels is similar. The magnitude and width of the pressure distribution increases as the net force level increases.

Subject 1: 1 inch Diameter Cylinder; ~50g, 75g, and 175g Net Force

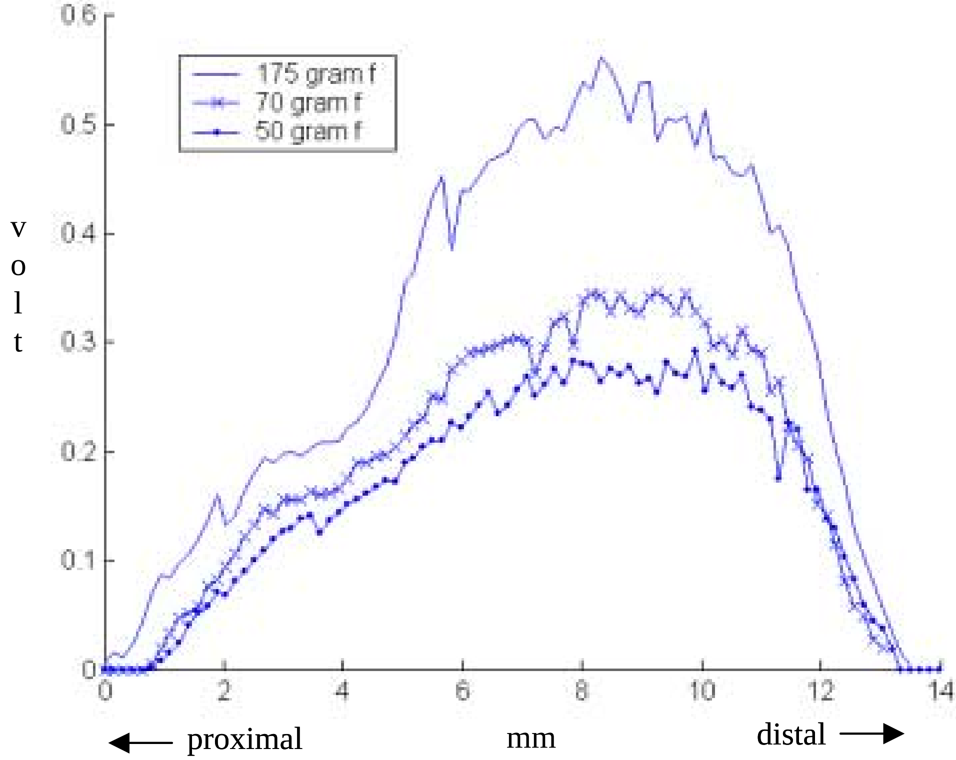

Figure 4-8. Pressure distribution measurement of subject 1 using a 1 inch cylinder with a load of 50 grams, 75 grams, and 175 grams.

Figure 4-9 shows the results of applying a net force of 24.5 grams, and 51.3 grams to the finger pad of subject 4 with the same ½ inch diameter cylindrical indentor. The general shape of the pressure distribution for both force levels is similar. The magnitude and width of the pressure distribution increases as the net force level increases.

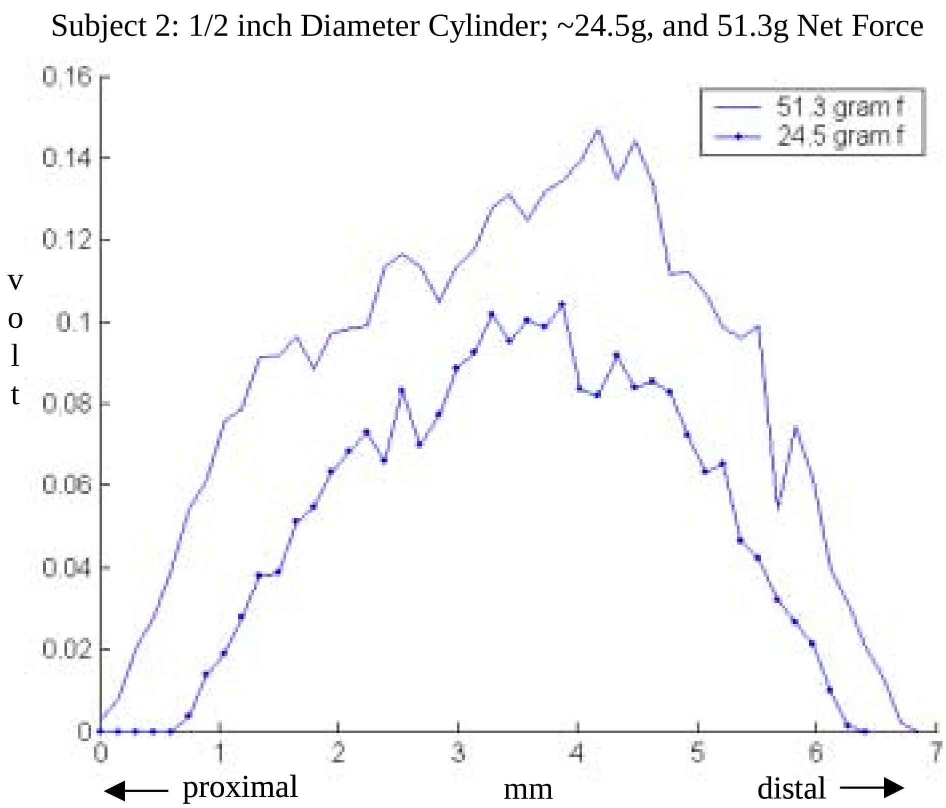

Figure 4-9. Pressure distribution measurement of subject 4 using a ½ inch diameter cylinder with a net force of 24.5 grams, and 51.3grams.

4.2.4 Finger Ridges

We were interested in the effects of varying the step size between samples. Figure 4-10 shows the results of applying a net force of approximately 150 grams to the finger pad of subject 1 with the 1 inch diameter cylindrical indentor for two different sample sizes. The samples were taken 0.3927mm apart and 0.2356mm apart. We can see that by taking the samples closer together, the spatial resolution of the measurements is increased.

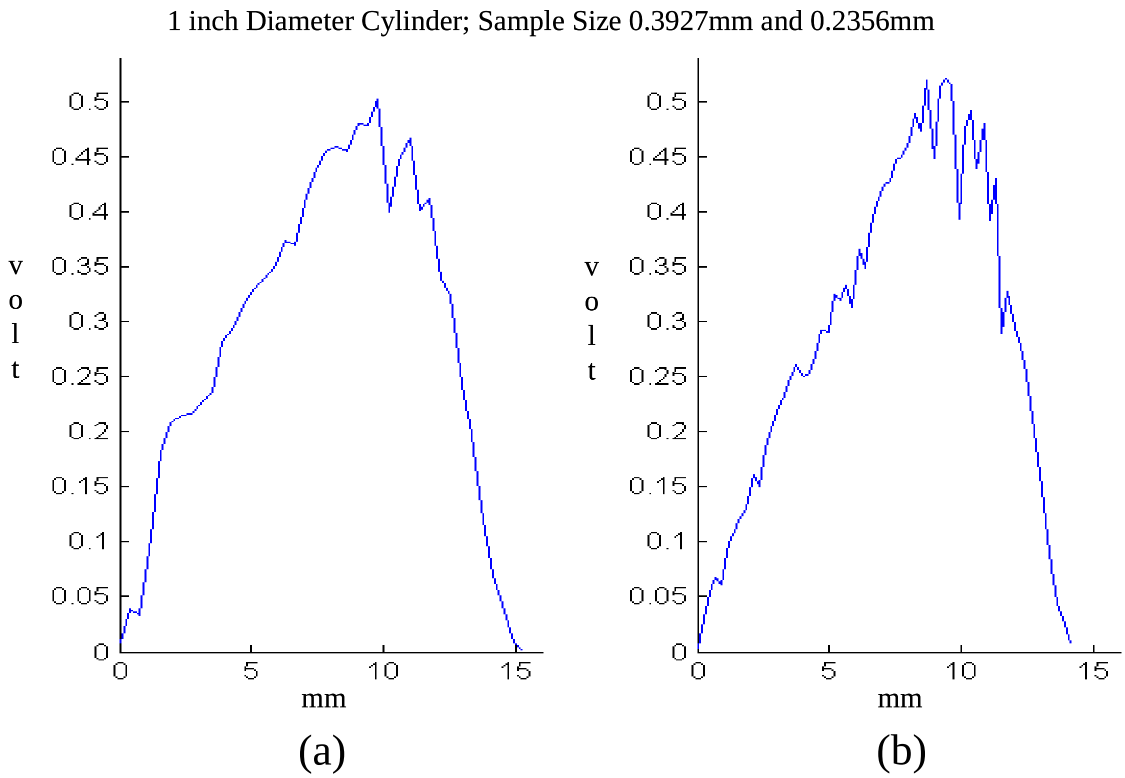

Figure 4-10. Pressure distribution measurement of subject 1 using a 1 inch cylinder with a net force of 150 grams. The samples were taken a) 0.3927mm apart and b) 0.2356mm apart.

Figure 4-11 shows the results of applying a net force of approximately 100 grams to the finger pad of subject 1 with the 1 inch diameter indentor. The samples were taken 0.03927mm apart. Although there is more apparent noise in the measurement, we can see that spatial resolution of the pressure measurement is enhanced, as the finger ridges seem to become more pronounced. However, comparison of the spatial response profile (Figure 3-19) to the data suggests that features less than ~1mm wide may be artifacts due to the bumpy spatial response profile of the sensor.

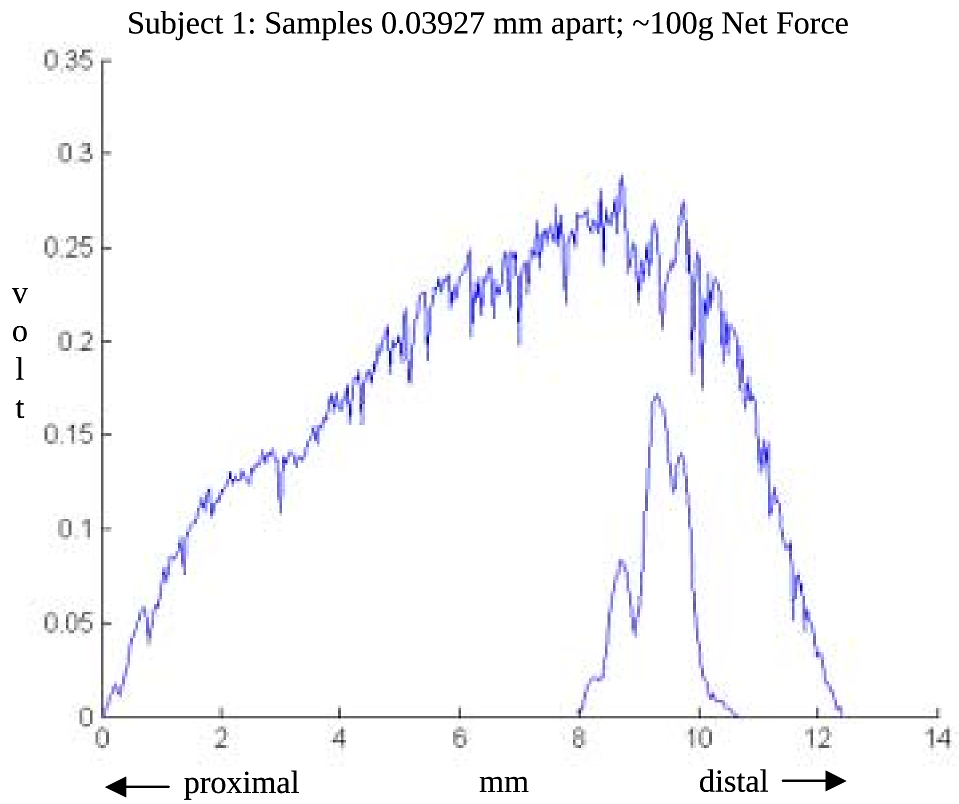

Figure 4-11. Pressure distribution measurement of subject 1 using a 1 inch cylinder with a net force of 100 grams. Samples were taken 0.03927mm apart. The spatial response profile of the pressure sensor is also plotted.

It would be useful to correlate these apparent finger ridges in the pressure measurement with the finger ridges in the finger pad. To investigate this correlation, we first took the pressure distribution measurements from the finger pad of subject 1, then wrapped a piece of paper around the sensor while it was attached to the indentor. We then applied ink to the subject's finger, and applied the indentor to the finger pad with the same total force used during the pressure distribution measurements. The resulting fingerprint, shown in Figure 4-12, was then used to correlate the possible finger ridges seen in the pressure distribution with the pattern of ridges on the subject's skin. Figure 4-13 shows the pressure distribution measurement along with lines that roughly correspond to the location of the grooves in the fingerprint.

Figure 4-12. Fingerprint of subject used to correlate with the possible finger ridges seen in the pressure distribution measurement.

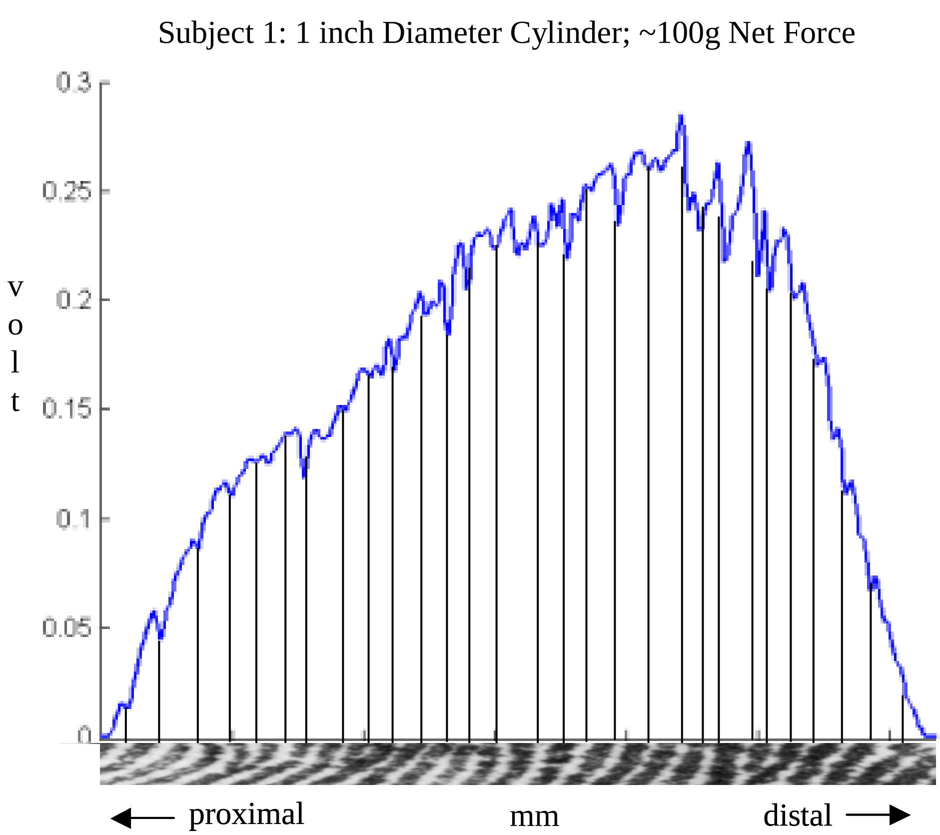

Figure 4-13. Pressure distribution measurement of subject 1 using a 1 inch cylinder with a net force of 100 grams. The lines correspond approximately to the location of the grooves in the fingerprint. The strip indicates the portion of the fingerprint scanned by the sensing element.

4.3 Comparison to Hertz Theory Predictions

Hertz theory (reviewed in Chapter 2) provides a rough approximation the fingerpad pressure distribution. Figure 4-14 compares the pressure distribution predicted by Hertz theory to pressures measureed under a 1 inch diameter cylinder exerting a net force of 56.1 grams. The magnitude and width of the Hertz pressure agree with observed values to within about 10% in the middle of the contact area, but fall off too quickly near the edges.

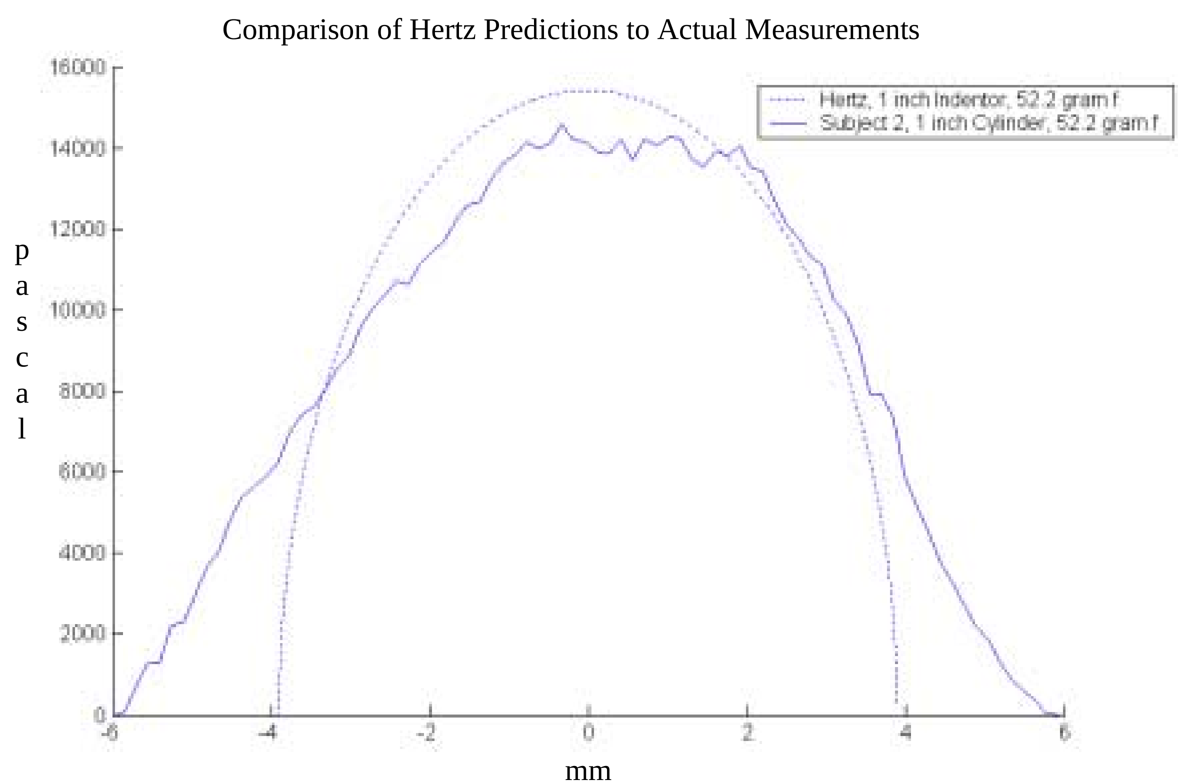

Figure 4-14. Comparison of the pressure distribution measured for a 1 inch diameter cylinder with a load of 56.1 grams (solid line) to the pressure distribution predicted by Hertz Theory (dashed line).

Figure 4-15 compares the pressure distribution predicted by Hertz theory to our pressure measurement for a ½ inch diameter cylinder and a load of 52.2 grams, and again the magnitude and width of the pressure measurement predicted by Hertz theory are relatively close to the observed pressure distribution. However, Hertz theory fails to model the observed asymmetry of the pressure distribution.

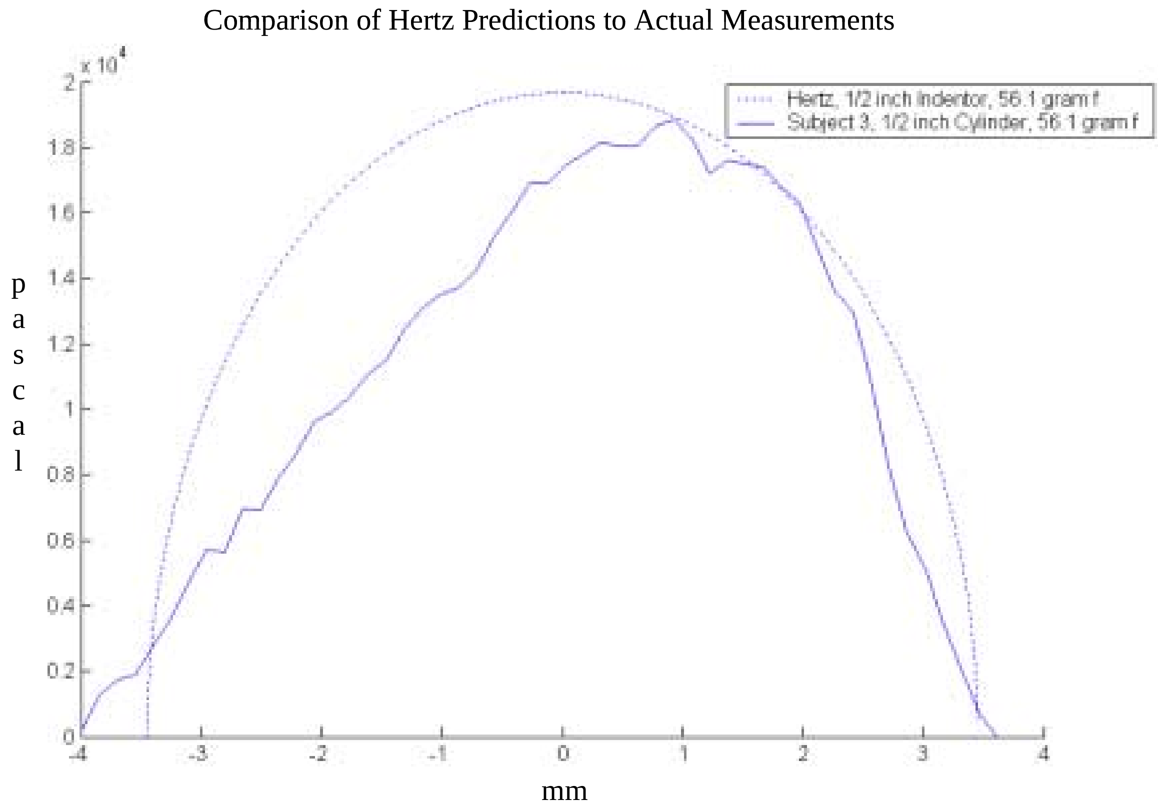

Figure 4-15. Comparison of the pressure distribution measured under a ½ inch diameter cylinder with a load of 52.2 grams (solid line) to the pressure distribution predicted by Hertz Theory (dashed line).

4.4 Deconvolution of Pressure Measurements

In order to compute the deconvolution of empirical pressure measurements, the spatial response profile of the pressure sensor was modeled as a Gaussian. Figure 4-16 shows the results of applying deconvolution to the pressure measurement result of subject 1 under a 100 gram net force. The spatial resolution of the pressure measurement was slightly increased as a result of the use of deconvolution, by assuming an unrealistically small standard deviation of 0.055 mm for the Gaussian. The general shape is the same but the magnitude of the peaks where finger ridges possibly appear in the pressure record is increased. Unfortunately, attempts to deconvolve the data using wider Gaussians with standard deviations closer to that observed in Figure 3-19 ($\sigma \cong 0.5$ mm), resulted in estimates of the pressure signal that were grossly in error. Using the raw spatial response profile shown in Figure 3-19 also produced poor results. Low pass filtering the data and spatial response profile did not fix the problem.

Subject 1: 1 inch Diameter Cylinder; ~100g Net Force; Measured and Deconvolved

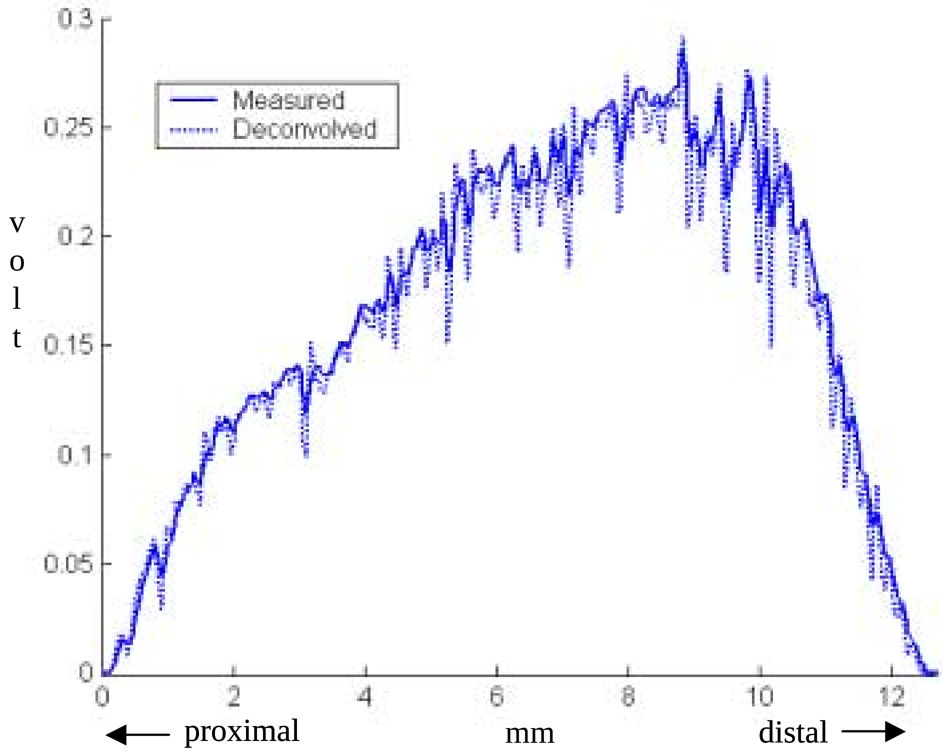

Figure 4-16. The measured (solid line) and deconvolved (dotted line) pressure distribution measurement for a 1 inch diameter cylinder with a net force of approximately 100 grams.

Figure 4-17 shows the results of applying deconvolution to the pressure measurements from subject 5 with a 50.8 gram load from a 1 inch diameter cylinder. The deconvolved signal appears to increase the spatial resolution of the pressure measurement. Again, the general shape and magnitude of the pressure distribution is the same after deconvolution is used. The magnitude of the peaks where finger ridges possibly appear in the pressure records is increased as well.

Subject 5: 1 inch Diameter Cylinder; ~50.8g Net Force; Measured and Deconvolved

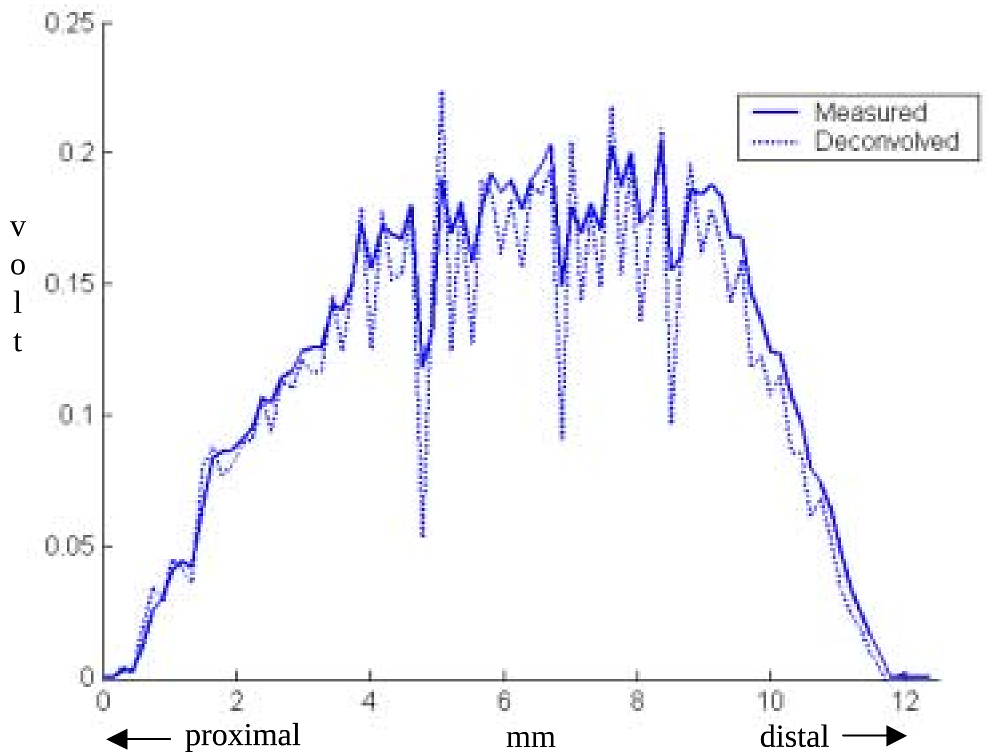

Figure 4-17. The measured (solid line) and deconvolved (dotted line) pressure distribution measurement for a 1 inch diameter cylinder with a load of 50.8 grams.

5.0 Summary

The surface pressure distribution of the finger pad is important because it is the input to the human tactile system. In this study we explored the relationship between the surface pressure distribution and the shape of contacting objects. We measured the pressure distribution on the surface of the finger in contact with an object using a highly sensitive pressure sensor. The effects of curvature and downward displacement on our surface pressure measurements were examined. We then used deconvolution to increase the spatial resolution of the empirical data.

A pressure measurement system was designed and built to measure the surface pressure of the finger pad. The behavior of the pressure sensor was examined to understand its characteristics and limitations. Drift, repeatability, linearity, anisotropy, inter-element variability, and the spatial response profile of the sensor elements were all measured. We showed that the sensor readings are approximately linear, anisotropic, and that the gain for each element of the sensor is different. The spatial response profile was measured and the sensor was calibrated in order to convert readings from voltage to pressure.

The surface pressure was measured from the finger pads of five subjects using both a 1 inch and ½ inch diameter cylinder under various loads. The spacing between samples was varied to see if a smaller step size between measurements produced better results. The correlation between pressure records and the fingerprint of one subject was explored. We found that the dips in the surface pressure record correlated approximately with the pattern of grooves in the finger print. The pressure records were compared with the pressure distribution as predicted by Hertz theory, and the overall shape and magnitude of the predicted and measured pressure distribution were found similar.

Deconvolution was used to increase the spatial resolution of the measurements. This enabled a slight increase in the spatial resolution of the pressure measurements, but not to the degree that was hoped for. This was most likely due to sensor noise, and the complexity of the spatial response profile.

References

Bicchi, A., Scilingo E., and Rossi, D., “Haptic Discrimination of Softness in Teleoperation: The Role of the Contact Area Spread Rate,” *IEEE Transactions on Robotics and Automation*, 16(5): 496-504, **October 2000**.

Birch, A.S. and Srinivasan, M.A., “Experimental Determination of the Viscoelastic Properties of the Human Fingerpad,” Touch Lab Report, *RLE Technical Report – 632*, MIT, **1999**.

Bloom, W. and Fawcett, D. *A Textbook of Histology*. W. B. Saunders Company, Philadelphia, pp. 563-580, **1975**.

Cysyk, J. “Skin Dynamics in the Tactile Sensing of Shape”, Dept. of Electrical Engineering, MIT September, **1999**.

Dandekar, K. and Srinivasan, M.A., “Role of Mechanics in Tactile Sensing of Shape,” Touch Lab Report 2, *RLE Technical Report – 604*, MIT, **1996**.

Darian-Smith, I. “The Sense of Touch: Performance and Peripheral Neural Processes,” *Handbook of Physiology – The Nervous System –III*, pp. 739-788, **1984**.

Diller, T. T., “Frequency Response of Human Skin in Vivo to Mechanical Stimulation,” S. M. Thesis., Dept. of Mechanical Engineering, MIT, **2001**.

Fearing, R.S. “Tactile Sensing Mechanisms,” *International Journal of Robotic Research*, 9:3-23, **1990**.

Fearing, R.S., and Hollerback, J.M., "Basic Solid Mechanics for Tactile Sensing," *International Journal of Robotic Research*, Vol. 4, No. 3, **Fall 1985**.

Goodwin, A. W., John, K. T., and Marceglia, A. H., "Tactile discrimination of curvature by humans using only cutaneous information from the fingerpads," *Experimental Brain Research*, vol. 86, pp. 663-672, **1991**.

Goodwin, A. W. and Wheat, H. E., "Human tactile discrimination of curvature when contact area with the skin remains constant," *Experimental brain research*, vol. 88, pp. 447-450, **1992**.

Gulati, R. and Srinivasan, M., "Determination of Mechanical Properties of the Human Fingerpad, *in vivo*, using a Tactile Simulator," *RLE Technical Report – 606*, MIT, **1996**.

Hajian, A. Z. and Howe, R. D., "Identification of the mechanical impedance at the human finger tip," *ASME Journal of Biomechanical Engineering*, 119(1), pp. 109-114, **February 1997**.

Ho, C. -H. and Srinivasan, M., "Human Haptic Discrimination of Thickness," *RLE Technical Report – 608*, MIT, **1996**.

Hodgkin, A. L. and Huxley, A. F., "A quantitative description of membrane current and its application to conduction and excitation in nerve," *Journal of Physiology*, pp. 117-500, **1952**.

Howe, R. S. and Cutkosky, M. R., "Dynamic Tactile Sensing: Perception of Fine Surface Features with Stress Rate Sensing," *IEEE Transactions on Robotic and Automation*, vol. 9, no. 2, pp. 140-151, **1993**.

Johansson, R.S. and Vallbo, A.B., "Tactile sensory coding in the glabrous skin of the human hand," *Trends in Neuroscience*, vol. 6, pp. 27-32, **January 1983**.

John, K. T., Goodwin, A. W., and Darian-Smith, I., “Tactual discrimination of thickness,” Experimental brain research, vol. 78, no. 1, pp. 62-68, **1989**.

Johnson, K.L. *Contact Mechanics*. Cambridge University Press, Great Britain, **1985**.

Karason, S. P., Annaswamy, A., and Srinivasan, M. A., “Identification and Control of Haptic Systems: A Computational Theory,” *RLE Technical Report – 621*, MIT, **1998**.

Karason, S. P., Srinivasan, M. A., and Annaswamy, A., “Encoding and Decoding of Static Information in Tactile Sensing Systems,” *The International Journal of Robotics Research*, vol. 18, no. 2, pp. 131-151, **February 1999**.

Karu, Z. Z., *Signals and Systems Made Ridiculously Simple*, ZiZi Press, Cambridge, Massachusetts, **1995**.

Lamb, G. D., “Tactile discrimination of textured surfaces: Psychophysical performance measurements in humans,” *Journal of Physiology (London)*, vol. 338, pp. 551-565, **1983**.

Lanir, Y., Dikstein, S., Hartzshtark, A., and Manny, V., “*In Vivo* Indentation of Human Skin,” *Journal of Biomechanics*, vol. 112, pp.63-69, **1990**.

Lederman, S. J. and Taylor, M. M., “Fingertip force, surface geometry, and the perception of roughness by active touch,” *Perception & Phychophysics*, vol. 12, pp. 401-408, **1972**.

Liao, J. C. and Srinivasan, M. A., “Experimental Investigation of Frictional Properties of the Human Finger Pad,” *RLE Technical Report – 629*, MIT, September, **1999**.

Lockhart, R. D., Hamilton, G. F., and Fyfe, F. W., *Anatomy of the Human Body*, JP Lippincott Co., Philadelphia, **1965**.

Maeno, T., Kobayashi, K, and Yamazaki, N., “Relationship Between the Structure of Human Finger Tissue and the Location of Tactile Receptors,” *JSME International Journal*, Series C, Vol. 41, No. 1, **1998**.

Pawluk, D. T. V., “A Visocelastic Model of the Human Fingerpad and a Holistic Model of Human Touch,” Ph.D. Thesis, Harvard University, May **1997**.

Pawluk, D. T. V. and Howe, R. D., “Dynamic contact of the human fingerpad against a flat Surface,” *ASME Journal of Biomechanical Engineering*, 121(6), pp. 605-611, **December 1999**.

Pawluk, D. T. V. and Howe, R. D., “Dynamic Lumped Element Response of the Human Fingerpad,” *ASME Journal of Biomechanical Engineering*, 121(2), pp. 178-184, **April 1999**.

Pawluk, D. T. V., Son, J. S., Wellman, P. S., Peine, W. J, and Howe, R. D., “A Distributed Pressure Sensor for Biomechanical Measurements,” *ASME Journal of Biomechanical Engineering*, 102(2), pp. 302-305, **April 1998**.

Phillips, J. R. and Johnson, K. O., “Tactile Spatial Resolution – III. A Continuum Mechanics Model of Skin Predicting Mechanoreceptor Responses to Bars, Edges and Gratings,” *J. Neurophysiology*, vol. 46, pp. 1204-1225, **1981b**.

Raju, B and Srinivasan MA, “Encoding and Decoding of Shape in Tactile Sensing,” Touch Lab Report 12, *RLE Technical Report - 630*, MIT, **1999**.

Son, J. S., *http://www.pressureprofile.com*

Srinivasan, M. A., “Surface Deflection of Primate Fingertip Under Line Load,” *J. Biomechanics*, vol. 22, no. 4, pp. 343-349, **1989**.

Srinivasan, M. A. and Dandekar, K. “An Investigation of the Mechanics of Tactile Sense using Two-Dimensional Models of the Primate Fingertip,” *J. Biomechanical Engineering*, vol. 118, pp. 48-55, **1996**.

Srinivasan, M. A. and LaMotte, R. H., “Encoding of Shape in the Response of Cutaneous Mechanoreceptors,” *Information Processing in the Somatosensory System*, Franzen and Westman, Wenner-Gren International Symposioum Series, MacMillan Press, pp. 59-69, **1991**.

Srinivasan, M. A. and LaMotte, R. H., “Tactual Discrimination of Softness,” *J. Neurophysiology*, vol. 73, no. 1, pp. 88-101, **1995**.

Srinivasan, M. A., Whitehouse, J. M, and LaMotte, R. H., “Tactile detection of slip: Surface microgeometry and peripheral neural codes,” Journal of Neurophysiology, vol. 63, no. 6, pp. 1323-1332, **1990**.

Tregear, R. T., *Physical Functions of Skin*, Academic Press, New York, **1966**.

Tubiana, R., *The Hand*, W.B. Saunders Company, Philadelphia, **1981**.

Voss, K.J. and Srinivasan, M.A., “Investigation of the Internal Geometry and Mechanics of the Human Fingerpad, *in vivo*, using Magnetic Resonance Imaging,” Touch Lab Report 10, *RLE Technical Report – 622*, MIT, **1998**.

Williams, P.L., *Gray’s Anatomy*, Churchill Livingstone, New York, pp. 375-398, Third Edition, **1995**.